Synthesis and characterizations of Cu doped ZnO/Ag_3PO_4 composite for methylene blue dye degradation from aqueous solution

Wegene Lelisa Beyecha

A thesis Submitted to the Department of Materials science and Engineering,

And School of Mechanical, Chemical and Materials engineering

Presented in Partial Fulfillment of the Requirement for the Degree of Master's in Materials science and Engineering

Office of Graduate Studies

Adama Science and Technology University

July 2021

Adama, Ethiopia

Synthesis and characterizations of Cu doped ZnO/Ag_3PO_4 composite for methylene blue dye degradation from aqueous solution

Wegene Lelisa Beyecha

Advisor: Gebisa Bekele Feyisa (Ph.D)

Co-advisor: Temesgen Debelo Desissa (Ph.D.)

A Thesis Submitted to The Department of Materials Science and Engineering

School of Mechanical, Chemical, and Material Engineering

Presented in Partial Fulfillment of the Requirement for the Degree of Master's in Materials Science and Engineering

Office of Graduate Studies

Adama Science and Technology University

July 2021

Adama, Ethiopia

DECLARATION

I hereby declaring that this Master Thesis entitled "**Synthesis and characterizations of Cu doped ZnO/Ag_3PO_4 composite for methylene blue dye degradation from aqueous solution** "is my original work. That is, it has not been submitted for the award of any academic degree, diploma, or certificate in any other university. All sources of materials that are used for this thesis have been duly acknowledged through citation

Name of the Student	Signature	Date

RECOMMENDATION

I/we, the advisor(s) of this thesis, hereby certify that I/we have read the revised version of the thesis entitled "**Synthesis and characterizations of Cu doped ZnO /Ag_3PO_4 composite for methylene blue dye degradation from aqueous solution**"prepared under my/our guidance by **Wegene Lelisa Beyecha** submitted in partial fulfillment of the requirements for the degree of Masters of Science in Materials Science and Engineering, Therefore, I/we recommend the submission of a revised version of the thesis to the department following the applicable procedures.

Major Advisor	Signature	Date
Co-advisor	Signature	Date

APPROVAL SHEET

I/we, the advisors of the thesis entitled "**Synthesis and characterizations of Cu doped ZnO/Ag_3PO_4 composite for methylene blue dye degradation from aqueous solution**" and developed by **Wegene Lelisa Beyecha**, hereby certifying that the recommendation and suggestions made by the board of examiners are appropriately incorporated into the final version of the thesis.

Major Advisor	Signature	Date
Co-advisor	Signature	Date

We, the undersigned, members of the Board of Examiners of the thesis by **Wegene Lelisa Beyecha** have read and evaluated the thesis entitled "**Synthesis and characterizations of Cu doped ZnO/Ag_3PO_4 composite for methylene blue dye degradation from aqueous Ssolution**" and examined the candidate during the open defense. This is, therefore, to certify that the thesis is accepted for partial fulfillment of the requirement of the degree of Master of Science in Materials Science and Engineering**.**

Chairperson	Signature	Date
Internal Examiner	Signature	Date

External Examiner Signature Date Finally, approval and acceptance of the thesis are contingent upon submission of its final copy to the Office of Postgraduate Studies (OPGS) through the Department Graduate Council (DGC) and School Graduate Committee (SGC).

Department	Head Signature	Date
_____	_____	_____
School Dean	Signature	Date
_____	_____	_____
Office of Postgraduate Studies,	Dean Signature	Date

ACKNOWLEDGEMENT

First of all, I would like to thanks my almighty God for helping me to realize my long dream, without the help of God, I would not be finished my work. Following I would like to extend my gratitude to my family for their unconditional support during this long journey. I have a great thanks to my advisor Dr.Gebisa Bekela Fayisa for encouraged, initiated, guided me during my thesis work. I would like to extend my thanks to my Co. Advisor Dr. Temesgen Debelo Desissa gave me constructive comments, encouraging me, and help me to finish my work on time. To all lab assistance in our department thank you for your support, special great thanks to Mr.Demeke for his unlimited support ,and I would like to thanks the Department of Material Science and Engineering. Lastly ,but not a least I would like thanks Adama Science and Technology University under the number (ASTU/SM-R/215/21) ,Adama,Ethiopia for funding and offering such a great scholarship to hold my master's program.

TABLE OF CONTENTS

Title **page**

LIST OF TABLES

LIST OF FIGURES

LIST OF ACRONYMS /ABBREVIATIONS

AOPS = Advanced Oxidation Process

CZ-0.5 =0.5% Cu doping ZnO

CZ-1 =1% Cu doping ZnO

CZ-2 =2% Cu doping ZnO

CZ-3 =3% Cu doping ZnO

CZ-4 =4% Cu doping ZnO

2.5(CZ-1)/A =2.5 % CZ-1 decorated on the surface of Ag_3PO_4

5(CZ-1)/A=5% CZ-1 decorated on the surface of Ag_3PO_4

10(CZ-1)/A=10% CZ-1 decorated on the surface of Ag_3PO_4

CR=Congo Red

DTA=Differential Thermal Analysis

ECB=Conduction band Edge

EVB= Valance Band Edge

Eg =Bandgap

FT-IR = Fourier Transform Infrared

MB =Methylene Blue

MO =Methylene Orange

MR = Methylene Red

PL =Photoluminescence spectroscopy

RhB =Rhodamine B

ROS =Reactive Oxygen Species

SEM=Scanning electromicroscopy

TGA =Thermal Gravimetric Analysis

UV-Visible (DRS) =Ultra-Violet -visible diffuse reflectance spectroscopy

XRD = X-ray Powder Diffraction

ABSTRACT

Water is contaminated by various dyes that toxic to living things .Photocatalysis essential to remove this dyes from wastewater. Ag_3PO_4 is a good candidate for the degradation of dyes in wastewater. However, the photocatalytic activity of Ag_3PO_4 is limited due to photo corrosion, instability issues, and a high recombination rate. In this work, $y(Zn_{1-x}Cu_xO)/z(Ag_3PO_4)$ composites were synthesized by in situ precipitation where y=2.5,5,10% and z=97.5,95,90% followed by characterizations using XRD,UV-Visible diffuse reflectance spectroscopy (UV-DRS), photoluminescence spectroscopy (PL), FT-IR, and thermal analysis by (TGA and DTA), Scanning electron microscopy(SEM). The peak of Cu doped ZnO was not observed on the XRD of the composites because of its small amount. The formation of the composite was confirmed by FT-IR peaks of Ag_3PO_4 shift from $1003cm^{-1}$ to $989cm^{-1}$ in the composite. The band gap of Cu doped ZnO and ZnO was calculated from UV-DRS data and found that 3.24eV and 3.24eV. The PL spectrum of composite showed lower intensity which indicates a lower recombination rate of charge carrier than Cu doped ZnO and Ag_3PO_4. The removal efficiencies of the composite, $Zn_{1-x}Cu_xO$, and Ag_3PO_4 were evaluated by UV-Visible spectroscopy. The optimum degradation of methylene blue from aqueous solutions using $Zn_{1-x}Cu_xO$ and $y(Zn_{1-x}Cu_xO)/ z(Ag_3PO_4)$ was observed at x=0.01,y=0.05 and z=0.95.Then, the removal efficiency of $Zn_{0.99}Cu_{0.01}O$ was 88% as compared with that of pristine ZnO because it has small particle size. the maximum degradation efficiency of the composite was observed at a pH value of 10 was 95% and at catalyst dose of 0.0444g/l was 97%. The degradation efficiency of $0.5(Zn_{0.99}Cu_{0.01}O)/0.95(Ag_3PO_4)$ composite was 94% greater than that of $Zn_{0.99}Cu_{0.01}O$ of 88% and greater than that Ag_3PO_4 of 82% because the recombination rate was reduced significantly and it was stable when it used for three-round test . Therefore, $0.5(Zn_{0.99}Cu_{0.01}O)/0.95(Ag_3PO_4)$ composites are a promising candidate material for the removal of methylene blue from aqueous solution.

Keywords: Cu-ZnO/Ag_3PO_4, Photocatalysis, MB (Methylene blue), Degradation, composite

CHAPTER ONE

1.INTRODUCTION

1.1. Background

In the twenty-one century, it is common to hear the news about environmental pollutions including air pollution, soil pollution, water pollution, and its severe consequence in terms of the economic, social, and political context. Among these pollutions, water pollution is one of the abundant pollutions which is detrimental to the health of people and ecosystem in the worldwide. Amazingly, air pollution, as well as soil pollution, indirectly resulted in water pollution. In addition to this, industrialization, urbanization, and dramatically increase in the population of the world are the main direct causes of water pollution(Martinez-Huitle and Brillas 2009).

Wastewater is classified into domestic, commercial, and institutional wastewater based on its origin. Domestic wastewater is the wastewater from residential activities like food preparation, laundry, cleaning, and personal hygiene, and commercial (industrially) wastewater is wastewater from the manufacturing industry (metal industry, textile industry pharmaceutically industry) and commercial activities such as printing, food, and beverage processing. Institutional wastewater is wastewater from large institutions like hospitals, universities, and educational facilities(Mathew, Rosary et al. 2016). All these wastewater mainly contains heavy metals like mercury ions, lead ions, chromium ion, arsenic ion, cadmium ions (Zhou, Yang et al. 2020), and various types of dyes and pathogens.

Over 100,000 types of dyes and more than 7×10^5 are annually produced which are released into water (Guivarch, Trevin et al. 2003). For instance some of dyes are methylene orange (MO),Methylene blue(MB) ,rhodamine B(RhB), methylene red(MB) ,congo red (CR) ,orange G (Nyankson and Kumar 2019).These dyes are used in tanning ,textile ,painting ,printing, cosmetics ,pharmaceutical ,paper making, leathery industries etc (Konstantinou and Albanis 2004). These dyes are very toxic to humans and they may cause different types of diseases like skin irritation, eye irritation, carcinogenic, typhoid, cholera, tuberculosis, heart attacking disease, and so on (Liu, Fu et al. 2011). To keep the health of the communities, it is essential to degrade or remove the dyes from wastewater. There are many remediation strategies

have been available to remove organic dyes and inorganic pollutants from wastewater. These water purifying techniques are summarized in Fig.1.1 as shown below.

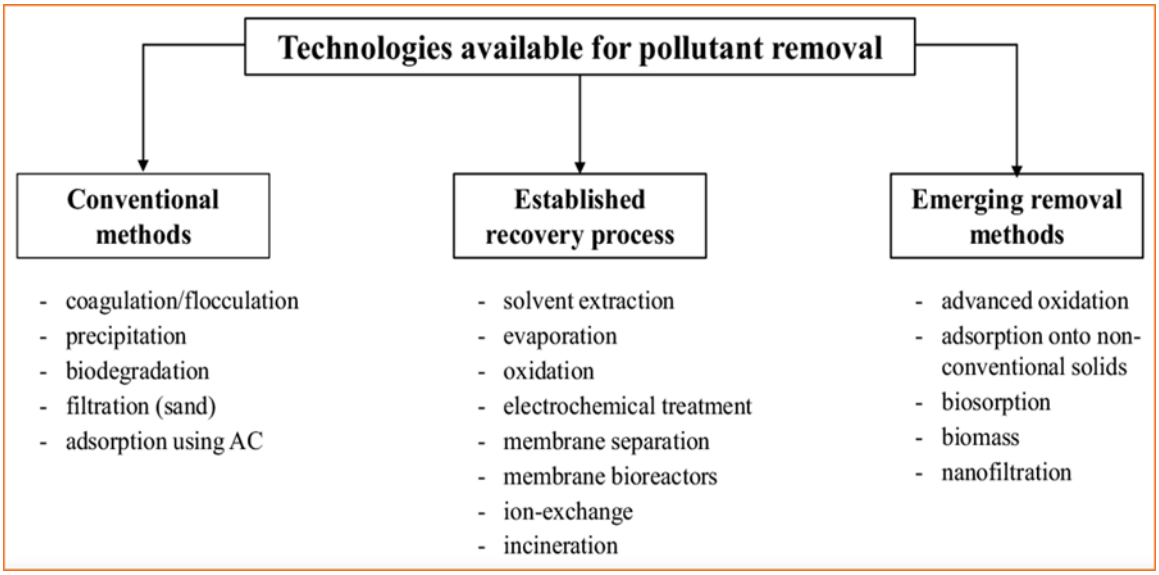

Figure :1.1 .Technologies are available for wastewater treatment(Deng and Zhao 2015).

Among the available technologies for wastewater treatment mentioned in Fig 1.1, advanced oxidation processes (AOPs) are effective in degrading non-biodegradable, chemically stable, and persistent organic pollutants because they produce reactive oxygen species that oxidizes and degrades the organic dyes. In addition to these, AOPs are low operating cost, no chemical agent needed, minimal sludge formation, and no needs maintenance(Miklos, Remy et al. 2018, Nyankson and Kumar 2019, Homlok, Kiskó et al. 2021). However, the other techniques did not effective for removing pollutants from wastewater because they are introducing secondary pollutants after removing a pollutant. For example, solid sludge settles in the bottom part of water. The common types of AOPs are photocatalysis, photolysis, and photo-Fenton (Elhalil, Elmoubarki et al. 2018, Martínez-Costa, Rivera-Utrilla et al. 2018). These methods are electrochemical oxidations based methods and, in all types of AOPs, reactive oxygen species (ROS) can be generated ,andthey can easily oxidize a broad range of organic pollutants in the water (Deng and Zhao 2015). Recently a semiconductor-based photocatalyst is an active area of research because of its effectiveness for photodegradation at a very low amount, no needs external force, environmentally benign and cost-effective technology, no introducing secondary pollutants in the system (Karimi, Zohoori et al. 2014, Dodoo-Arhin, Buabeng et al. 2018). The schematic mechanism photocatalyst is shown in Fig 1.2. First, the semiconductors

materials irradiated by the light source of energy greater than or equal to band gap absorbed and exciting electron from valance band to conduction band by leaving holes in the valance band. The creating holes and electrons form reactive oxygen species (ROS). The ROS attack organic dyes and decomposed them into harmless compounds such as H_2O, CO_2, and other non-toxic by-products (Shan, Ghazi et al. 2010, Zhang, Li et al. 2015).

.

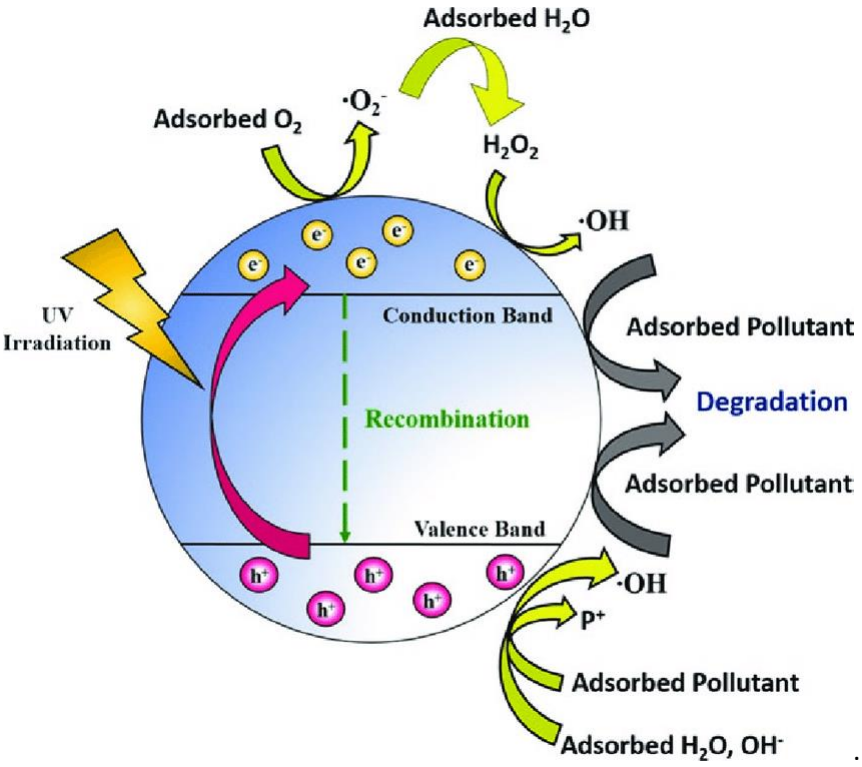

Figure: 2.1 .Schematical mechanism of the photocatalyst(Adam, Pozina et al. 2018)

TiO_2 and ZnO are major semiconductors used as photocatalyst oxide material due to the possess good photo and chemical stability, cheaper and it has high oxidation power for a decomposing broad range of organic pollutant (Fujishima and Honda 1972). Comparing TiO_2 to ZnO, ZnO has high oxidation power holes and removes diversity of organic pollutants and high absorption of solar light than TiO_2 due to the position of the valance band of ZnO (Miyauchi, Nakajima et al. 2002). The ZnO has a direct bandgap of 3.32-3.37eV at room temperature, and an n-type semiconductor with a small exciton binding energy of 60 meV (Alaria, Turek et al. 2005, Sluiter, Kawazoe et al. 2005). Naturally, half of ZnO tetrahedral has unfilled voids of wurtzite structure, so controlling of ZnO inherent is defects extremely essential

for controlling its properties. However, ZnO has large band gaps (3.2- 3.37 eV) which allowed them to operate under UV-light, but the UV light reaches the earth's surface only 3-5%, but the visible light reaches the earth surface 45-48%(Pirhashemi and Habibi-Yangjeh 2014). The high recombination of photogenerated charge carriers also suppressed the photocatalytic activity ZnO.

Thus, recently the materials operated under visible light have been gaining great attention than materials worked under UV light. Two approaches to solving the above issue :(i) improving the photocatalyst activity ZnO by doping and coupling within small bandgap semiconductor. The most common transition metals used as dopant of ZnO are Al, Cu,Fe,Co,Ni,V,Si ,Mn ,etc (Kim, Kim et al. 2012, Jeyachitra, Senthilnathan et al. 2017, Simimol, Anappara et al. 2017, Chandekar, Shkir et al. 2020).The doping can reduce the bandgap to extend solar light absorption in a longer wavelength region. This was justified by observing optical redshift absorption of ZnO by doping transition metals due to the sp-d interaction of the band electrons and the localized d-electrons of M^{++} transition metals substituted for Zn^{++} ions (Kim, Kim et al. 2012, Beltrán, Barrero et al. 2016), which attributed to the negative and positive shift of valance and conduction band, respectively. This leads to the shrink of the band gap (Kim and Park 2002).

Cu metal was the most essential dopant of ZnO because it can modify the luminescence of ZnO crystals by introducing impurity levels, and it has the same physical and chemical properties as Zn. coupling ZnO with small bandgaps such as Fe_2O_3, WO_3, Ag (F, I), SnO_2, Bi_2O_3, CuO, Cu_2O, Ag_3PO_4, etc also improves its photocatalytic activities (Wu, Cao et al. 2009, Yi, Ye et al. 2010, Katsumata, Oda et al. 2013, Sun, Zhu et al. 2016, Serrà, Gómez et al. 2020). (ii) The second approach searching for the material driven by visible light such as Ag_3PO_4,g-C_3N_4, WO_3, CuO, Bi_2O_3 $BiWO_4$ (Du, Song et al. 2021). Among these, Ag_3PO_4 has been highly absorbing solar light (it has quantum efficiency up to 90%), its indirect bandgap, n-type semiconductor, and has a forbidden gap width of 2.45 eV. However, the photocatalytic activity of Ag_3PO_4 has been limited by low thermal stability, low chemical inertness, photo corrosion (the Ag^+ in Ag_3PO_4 is easily reduced to elemental silver (Ag°) by photogenerated electron) which prevented light absorption, and high recombination of charge carriers (Chen, Liu et al. 2017, Zhu, Hu et al. 2020). So far, many methods have been proposed to alleviate the limitation

of Ag_3PO_4, some of them are the following: decorating the Noble metals on it, coupling it with organic materials such as graphene (Xiang, Lang et al. 2015), rGO, cellulose (Lebogang, Bosigo et al. 2019), and g-N_3C_4 (Zhang, Lv et al. 2017), coupling it with another semiconductor-based material such as Fe_3O_4, CuO, Co_3O_4, ZnO, AgBr, AgCl, and changing calcination temperature (Chen, Liu et al. 2017, Chen, Zhao et al. 2018, Guo, Shi et al. 2018, Martín-Gómez, Navío et al. 2020). For instance, ZnO/ Ag_3PO_4 reduces the photo corrosion, instability of Ag_3PO_4 (Luo, Xu et al. 2015, Zhu, Duan et al. 2020). However, ZnO is not activated by visible light and the combination of two semiconductors n-ZnO/n-Ag_3PO_4 which more or less hinder the performance of the photocatalytic activity.

Therefore in this work, Cu doped ZnO coupled with Ag_3PO_4 were synthesized for the degradation of organic dyes. It is shown that Cu doped ZnO/ Ag_3PO_4 composite shows better photocatalytic activities than Cu doped ZnO and Ag_3PO_4 due to its bandgap modification. These Cu dopedZnO/Ag_3PO_4 was synthesized by in situ precipitation technique. The crystallinity, phase purity, morphology, optical property, the bond between atoms, thermal property were determined by XRD, SEM, UV-Visible diffuse reflectance spectroscopy (UV-DRS), PL, FTIR, TGA, and DTA. The experimental results revealed that the composite is a promising material for the degradation of dyes.

1.2. Problem of statement

Water is contaminated with organic dyes that are dangerous or toxic to humans and animals. To keep and save a life, removing dyes from wastewater is crucial. There are various water treatment technologies used for removing organic dyes from wastewater such as coagulation, sedimentation, reverse osmosis, membrane filtration, adsorption, advanced oxidation process (Rout, Zhang et al. 2021). The advanced oxidation process preferable over the others due to its low toxicity, degrading dissolved organic pollutants, and chemical stable organic contaminants, low operating cost, no chemical agent needed so that it minimizes sludge formation (Ma, Yi et al. 2021).

From the types of AOPs a photocatalysis is indispensable than others owing to a cost-effective, very small quantity of photocatalyst is effective for degradation, it can work under solar radiation for degradation of toxic pollutants, and it does not need external force (Nyankson and Kumar 2019). Semiconductors photocatalyst are Cu_2O, CuO, Ag_3PO_4, ZnO, TiO_2, WO_3,

Co_3O_4, and Sb_3O_5. Among these, Ag_3PO_4 is preferable because of its high absorbance of visible light. However, the photocatalytic activities of Ag_3PO_4 were limited due to photo corrosion, unstable, and the recombination of the charge carriers. Therefore, to mitigate the limitation of Ag_3PO_4, coupling it within semiconductors such as ZnO was reported (Luo, Xu et al. 2015, Zhu, Duan et al. 2020), but zinc oxide did not work under visible light, so Cu doped ZnO can reduce its bandgap to visible light range absorbance and reduce the barrier between ZnO and Ag_3PO_4. Hence, Cu doped ZnO in the composite plays a prominent role in enhancing the photocatalytic activities of the composites.

1.3. Objective of the study

1.3.1. Generally objective

Synthesis and characterizations of Z/Ag_3PO_4 composite for methylene blue dye degradation from aqueous solution.

1.3.2 Specific Objective

- Synthesizing $Zn_{1-x}Cu_xO$ (x= 0, 0.005, 0.01, 0.02, 0.03, 0.04) using precipitation techniques
- Optimizing the composite y($Zn_{0.99}Cu_{0.01}O$)/z(Ag_3PO_4) (y=0% ,2.5%,5%,10 % and z=97.5,95,90%) by checking its photocatalytic activities
- Characterizing the synthesized materials by using XRD, SEM, PL, UV –visible DRS spectroscopy, FTIR
- Investigating the effect of calcination temperature on the photocatalytic activity of Ag_3PO_4
- Scrutinizing the photocatalytic activity of synthesized material
- Investigating the effect of the catalyst dosage and pH values on the degradation of methylene blue.

1.4. Scope of the studies

This study covers facile synthesis of single component Cu doped ZnO, Ag_3PO_4 by precipitation method, and synthesized of binary Cu doped ZnO/Ag_3PO_4 composite by a low-cost technique called in situ chemical precipitation methods. Furthermore, the

photodegradation of the Methylene blue (MB) from aqueous solution by single component and binary composite and the effect of calcination temperature on Ag_3PO_4 photocatalytic activity have been investigated.

1.5. Significance of the study

The degree of water pollution is more than words because as the technologies have been advanced, and the amounts of the discharged wastes to the environment increase which directly or indirectly affect the quality of the water. Particularly in the countryside, getting treated water is unexpected as a result water-borne diseases are largely widespread. Finding a cheap and available method for these communities is significantly important. Therefore, Cu doped ZnO/ Ag_3PO_4 composite is cheap and can be easily synthesized, so that it can be considered as a potential wastewater treatment semiconductor photocatalyst in cities as well as in the countryside's area. In addition to this, Cu doped ZnO/ Ag_3PO_4 is a promising material for energy production, carbon dioxide reduction, and gas sensors.

CHAPTER TWO

2.LITERATURE REVIEW

2.1. Introduction

Environmental pollution including air pollution, soil pollution, and water pollution have serious consequences on the life of human beings and other organisms (Wei, Van Le et al. 2021). Air pollution has been caused by the combustion of fossils fuels, biomass, and automobile exhaust (Khomenko, Cirach et al. 2021, Maione, Mocca et al. 2021). Similarly, the degradation of land due to the presence of chemicals or other man-made substances in the soil causes soil pollution. The final destination of air and soil pollution is in the water body so that they can cause water pollution indirectly. In addition to these, the release of detergents and sewage, agricultural wastes (i.e. fertilizers and pesticides), solid wastes, and industrial wastes (i.e.toxic substances like dyes, grease, acids, oils, and heavy metal discharged) are often discharged to lakes, sea, rivers, oceans, ponds, streams water and so on. As a result water quality can significantly deteriorate.Though about three-fourths of the Earth's surface covered with water bodies. However, the availability of fresh water for living things is limited due to the pollution of water (Wei, Van Le et al. 2021).

2.1.1 Sources of wastewater and its consequences

The enormous expansion of the industries such as textile industry, pharmaceutical industry, metal industry, painting industry, manufacturing industry, sugar industry, and mining industry are significant discharge waste materials which cause water pollution. Some of the discharged materials are inorganic, organic, and pathogens. Examples of inorganic pollutants are Cd, Cr, Fe, Pb, Hg, Ni, and Zn (Sörme and Lagerkvist 2002, Barakat 2011, Egbueri 2020) are discharged into water from metalworking, and electroplating industries. Organic pollutants are discharged from thermal power plants and chlorinated organics, dioxins, suspended solids discharged to the water from the paper mill, and pulp industries (Gunkel, Kosmol et al. 2006, Barakat 2011, Dwivedi, Mishra et al. 2018).In addition to this, agriculture activities such as agrochemicals, nutrients, organic matters, drug residues are also the main cause of water pollution(Evans, Mateo-Sagasta et al. 2019). Drinking contaminated water may cause hepatitis, cholera, dysentery, cryptosporidiosis, giardiasis, diarrhea, and typhoid and it is put people at risk of carcinogenic diseases (Li, Jing et al. 2021). Approximately, 2.3 billion people in the

world are affected by water-borne diseases, where more of the percentage have been shared by developing countries (Wang and Yang 2016). Using wastewater not only hurts a human being but also affects the growth of plants. For instance, in china production of rice decreased due to untreated industrial wastewater that can weaken the growth of roots, seedlings, and tillers(Sun, Pan et al. 2016).

Usually, textile industry firms discharged a large number of toxic dyes released into water which threatened the health of animals, humans, and the aquatic ecosystem, so treating the wastewater from the textile industry before discharge to water is essential for saving life(Amornpitoksuk and Suwanboon 2014, Chen and Carroll 2016).

2.1.2 Wastewater treatment methods

The commons wastewater treatment methods are coagulation/flocculation, filtration (sand), adsorption on AC, chemical precipitation, biodegradation, Solvent extraction, advanced oxidation process, adsorption onto non-conventional solids, biosorption, biomass adsorption, Nanofiltration (Hu, Yang et al. 2005, Aziz, Alias et al. 2007, Acharya, Sahu et al. 2009, Hollender, Zimmermann et al. 2009, Zahrim and Hilal 2013), and advanced oxidation process(AOPS). Currently, the advanced oxidation process (AOPs) is preferable because of its forming reactive oxygen species to degrade organic dyes and changed them into CO_2 and H_2O (Lee and Park 2013).

AOPs classified based on the light irradiated and non –irradiated as following: (1)non-light irradiated AOPs:- include cavitation, Fenton and Fenton-like processes, ozonation, ozone/hydrogen peroxide, wet air oxidation (2) light irradiated AOPs:- include homogeneous (UV/hydrogen peroxide, UV/ozone, UV/ozone/hydrogen peroxide, photo-Fenton, homo, and heterogeneous (photocatalysis) processes.

The photochemical or photodegrading using metal oxide-based semiconductor attracted the attention of many researchers for the environmental remediation and wastewater treatments due to the following advantages: Cost-effective, no sludge formation like other methods such as adsorption, coagulation, flocculation, not generate any other secondary pollutant, a very small quantity of photocatalyst is required for the treatment and its environmental appealing. Moreover, the selected catalyst possesses no toxicity to human (Parvulescu and Granger

2013)health. The process of degradation of dyes using metal oxide and the sunlight is known as photocatalysis (Luis Sánchez-Salas, Aguilar Ubeda et al. 2017).

2.1.2.1. Semiconductor based photocatalysis

Semiconductor-based materials used as photocatalysis for mineralization organic pollutants inside wastewater are ZnO (Meng and Juan 2008), WO_3 (Hepel and Hazelton 2005) ,Co_3O_4 (Yang, Wang et al. 2019), TiO_2 (Lee and Park 2013), Fe_3O_4 (Ruzmanova, Stoller et al. 2013), CuO (Behjati, Sheibani et al. 2020), Cu_2O (Su, Chen et al. 2021), Ag_3PO_4, (Ge, Zhu et al. 2012)and so on. Among this material, ZnO nanomaterial attracted the attention of many researchers due to, its low cost, easy availability e, producing high oxidative power holes and environmentally friendly, its exciton binding energy of up to 60 m eV, thermal stability, high chemical stability, photosensitive, and catalytic activity, suitable bandgap, rich and controllable morphology(Martínez-Costa, Rivera-Utrilla et al. 2018). However, the ZnO semiconductor is limited to UV light, but the UV light that reaches the earth's surface is only 3-5% while the visible light reaches the earth's surface 48 %.To mitigate this issue, recently researchers focus on two approaches:(i), doping with metals and coupling with another low bandgap semiconductor material. The most common transition metals doped for ZnO are Al, Cu, Fe, Co, Ni, V, Si, etc. For instance, many current studies show that doping is monitoring the magnetic, optical, electrical property by controlling defect density and defect centers found in the ZnO lattice(Jin, Fukumura et al. 2001, Simimol, Anappara et al. 2017, Ma, Ren et al. 2019).

Doping is reducing the bandgap to extend solar light absorption in a longer wavelength. Optical redshift absorption of ZnO by doping transition metals due to the sp-d interaction of the band electrons and the localized d-electrons of M^{++} transition metals substituted for Zn^{++} ions(Kim, Kim et al. 2012, Beltrán, Barrero et al. 2016), which attributed to the negative and positive shift of valance and conduction band respectively, this leads the shrink of band gap(Kim and Park 2002, Ma, Ren et al. 2019).

Thus, Cu was a most essential transition metal to doped the ZnO than others due to it is luminescence activator, which can modify luminescence of ZnO crystals by introducing impurity levels, it has many physical and chemical property which are similar to Zn, and it can effectively change the optical and microstructure of ZnO(Liu, Deng et al. 2008, Zhang, Yi et al.

2008, Tao, Ma et al. 2011)(ii), The second approach is searching for the material operated under visible light.

In 2011, Ye reported silver orthophosphate (Ag_3PO_4) which possesses high visible light photocatalysis activity. Especially, quantum yields up to 90% for oxygen evolution from water Splitting and organic pollutant degradation at wavelength >420nm (Yi, Ye et al. 2010, Umezawa, Shuxin et al. 2011). Ma and Co-workers reported the structural features of the Ag_3PO_4. The energy band structure and density of the state of the Ag_3PO_4 are mainly responsible for harnessing solar energy for oxidizing water and degrading pollutants inside wastewater. The crystal structure of Ag_3PO_4 embraces isolated, regular PO_4 tetrahedral with a P-O distance of ~1.539Å. The six Ag^+ ions dispersed among twelve sites of 2-fold symmetry shown in Fig 2.1. It belongs to the body-centered cubic (bcc) structure type with a lattice parameter of 6.004Å, and the space group is $P4\bar{3}n$(Al Kausor, Gupta et al. 2020).

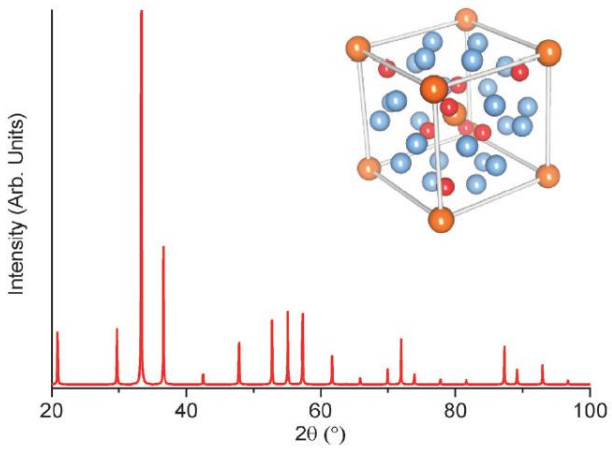

Figure:2.1 .XRD pattern for Ag_3PO_4 together with a simplified unit cell of Ag_3PO_4 (P– orange, O– red, Ag– blue) (Yi, Ye et al. 2010)

However, Some of the commons factors that hinder the photocatalytic activities of Ag_3PO_4 are photo corrosion, high recombination charge carriers, and Instability issues. To mitigate these, recently many researchers focus for exploration novel Ag_3PO_4 catalyst and develop the mechanism which improved photocatalysis stability of Ag_3PO_4 (Luo, Li et al. 2014, Zhang, Gu et al. 2015). In the next sub-sections, the possible method used to enhance the photocatalytic activities of Ag_3PO_4 will be discussed.

2.1.2.1.1. Working principle of photocatalysis

The photocatalytic reaction depends on the photon energy and catalyst. In general, semiconducting materials are used as a catalyst that performs as sensitizers for the irradiation of light stimulated redox process due to their electronic structure, which is characterized by a filled valence band and a vacant conduction band (Samsudin, Sze et al. 2015, Giovannetti, Rommozzi et al. 2016). Generally, the mechanism of photocatalysis for wastewater treatment is explained as follows in Fig 2.5. (1) the light (photon) energy which has energy greater or equal to bandgap is irradiated on the surface of catalyst (2) Electron excited from valance band to conduction band by leaving a hole in CB (3) The electron in CB reduced the oxygen in aqueous solution and form super radicals oxygen and hole reacted with hydroxide ions and water form hydroxide radically (4) Finally, holes, the superoxide and hydroxide radically oxidized pollutant into the non-toxic product like CO_2, H_2O. Besides this, the holes and electrons generated by irradiated light energy undergo successive oxidation and reduction reactions with any species, which might be adsorbed on the surface of the semiconductor to give the necessary products

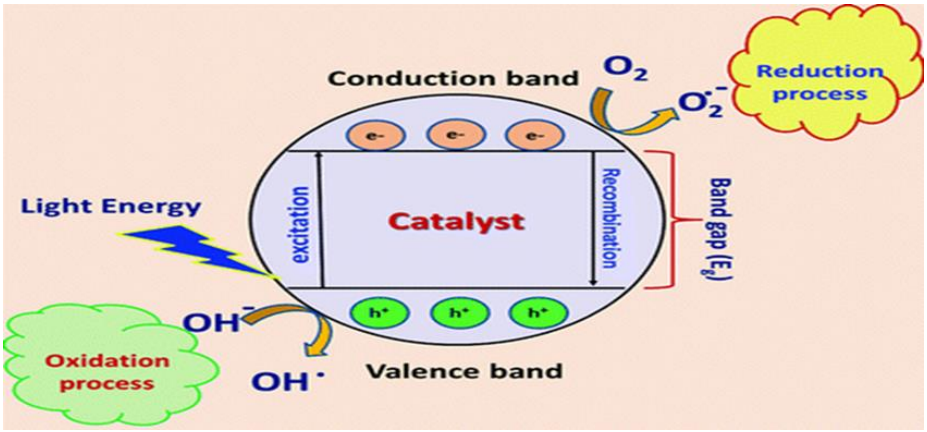

Figure:2.2.General mechanisms of photo catalysis(Saravanan, Gracia et al. 2017)

The oxidation reaction during the photodegradation of organic dyes takes place by holes. First, the dye molecule adsorption on the surface of the catalyst is achieved that could take place in the dark. Then, the photodegradation reaction could take place on the surface of the catalyst as follows in Fig.2.3.The holes formed in the VB could be trapped by H_2O, and oxidized H_2O into OH^- ions to generate °OH radicals. The generated °OH radicals reacted with dyes molecules in water and mineralizing it into CO_2, H_2O, and non-toxic minerals (Saravanan, Gracia et al. 2017)

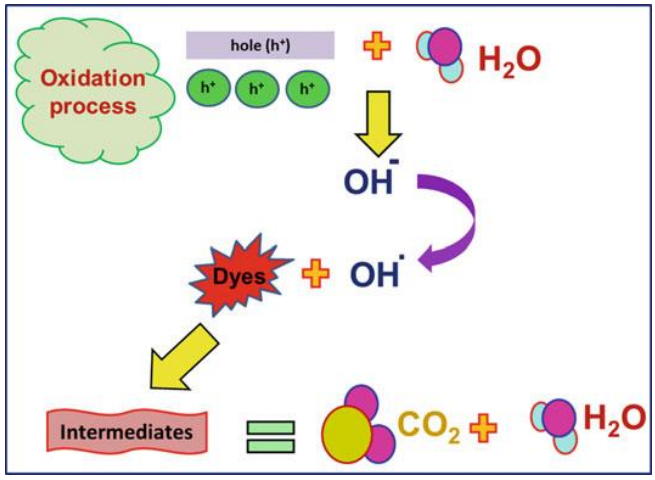

Figure:2.3. Representation of oxidation mechanism (Saravanan, Gracia et al. 2017)

Reduction reaction the reduction reaction during photodegradation of organic dyes proceed as following in Fig 2.4. First, the photogenerated electron in the conduction band of catalyst surface directly reacted with the oxygen adsorbed to surface catalyst formed $O°_2^-$, and $O°_2^-$ reacted with H^+ to produce °OOH and H_2O_2. Finally, $O°_2^-$, °OOH, and H_2O_2 mineralized the organic dyes into carbon dioxide and water.

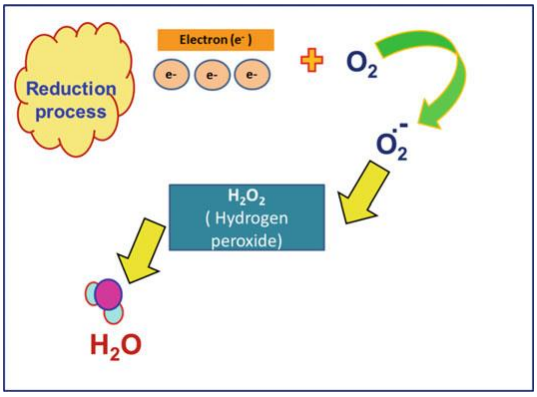

*Figure***:***2.4 .Representation of reduction reaction (Saravanan, Gracia et al. 2017)*

2.1.2.1.2.Possible methods for enhancing photocatalytic of Ag_3PO_4

2.1.2.1.2.1 .Calcination of Ag_3PO_4 at high temperature

Calcination of Ag_3PO_4 at high temperature is the alternative method of enhancing stability Ag_3PO_4 because it can modify the physicochemical properties of Ag_3PO_4 such as crystallinity, surface area, and the formation of oxygen vacancy which were responsible for enhancing photocatalytic activity of silver orthophosphate (Yu, Yu et al. 2003, Noda, Lee et al.

2008, Zhu, Neale et al. 2010, Lin, Guo et al. 2013, Tang, Liu et al. 2016). Ruifeng reported calcination of Ag_3PO_4 at 400 ºC reveals high photocatalytic activity toward degradation of methylene blue and oxygen evolution from water due to improved crystallinity, and formation of high oxygen vacancy when calcined at high temperature (Chong, Cheng et al. 2016). Calcination of Ag_3PO_4 helped to decorate Ag metals on the surface of Ag_3PO_4 without any photoreduction, which assists to suppress photo corrosion and enhance the stability of Ag_3PO_4 by accepting electron excited from valance band to conduction band, and also extending an absorption of the solar light in a long wavelength.

2.1.2.1.2.2. Loading nobles metal on the surface of Ag_3PO_4

The noble metal loaded on the surface of Ag_3PO_4 acts as an electron scavenger so that they can reduce the recombination rate and photo corrosion as shown in Fig.2.5. In other words, the excited electrons from the valence band are removed from the Ag_3PO_4 by noble metal so that there is no further recombination of electrons and holes. In addition to this, noble metal suppresses photo corrosion because the excited electron does not get Ag^+ ions in the solution to form black Ag^o metal that covers the active sites of Ag_3PO_4 (Yan, Zhang et al. 2014). Many reported works on the loading of noble metal on surface Ag_3PO_4 to enhance the photocatalytic activities of Ag_3PO_4 as shown in Table 2.1.

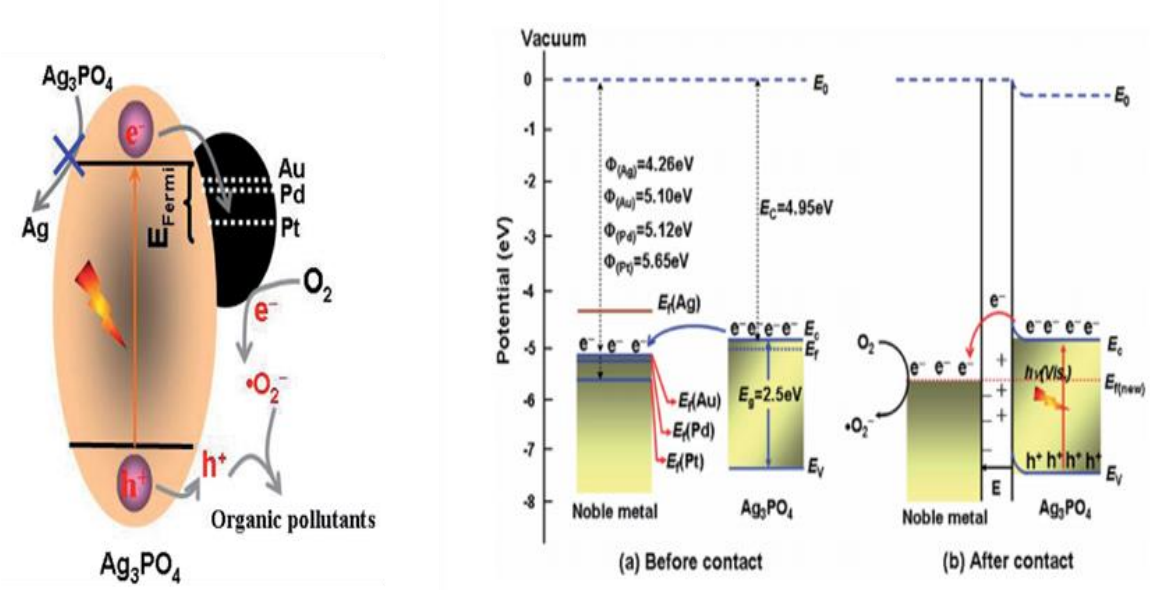

Figure:2.5. Mechanism of electron transfer between Ag_3PO_4 and noble metals(Yan, Zhang et al. 2014)

Table: 2.1.Summary of the reported on loading noble metal on the surface of Ag_3PO_4

Loaded noble metals	Types of dyes	Efficiency	Reference
Pt/Ag_3PO_4	MO	100%(15min)	(Yan, Zhang et al. 2014)
Au/Ag_3PO_4	MO	88%(15min)	(Yan, Zhang et al. 2014)
Pd/Ag_3PO_4	Mo	86(15min)	(Yan, Zhang et al. 2014)
Ag/Ag_3PO_4	RhB and MB	100%(40min)	(Teng, Li et al. 2012)
Ag/Ag_3PO_4	RhB	100%(20min)	(Bi, Hu et al. 2012)

Figure 2.2 shows the enhancement of photocatalytic activities of the Ag_3PO_4 by loading noble metals. Different noble metals have a different effect on enhancing photocatalytic activities of Ag_3PO_4 because of their various specific properties. Different noble metals loaded on Ag_3PO_4 shows unequal performances because they have not equal work functions. The large differences in work function between the noble metals and Ag_3PO_4 are necessary for a better photocatalytic process because it facilitates a transfer of a photogenerated electron from Ag_3PO_4 to noble metals. The efficiency of degrading dyes of Pt/Ag_3PO_4> Pd/Ag_3PO_4 >Au/Ag_3PO_4 because of their difference in work function. Wang, et al. reported that loading noble metals on the surface of Ag_3PO_4 improves the stability issue as well. Figure 2.6, shows loading platinum (Pt) on the surface of Ag_3PO_4 to enhance the stability and durability of the Ag_3PO_4 (Yan, Zhang et al. 2014).

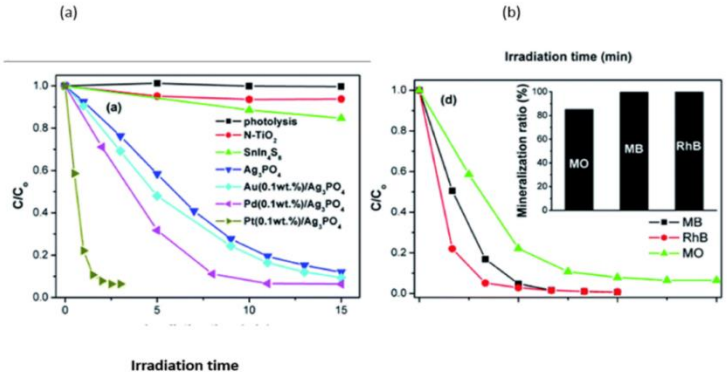

Figure:2.6 .a) Photocatalytic degradation curves of MO by Pt/Ag_3PO_4 (Yan, Zhang et al. 2014).

2.1.2.1.2.3 . Forming binary Ag_3PO_4 composite with semiconductor and support material

The main intentions to form heterojunction between metal oxides or supporting materials and Ag_3PO_4 are: (I) to solve instability issues, (ii) reducing the photo corrosion, (iii) improving the absorption of solar light in the visible range(Yi, Ye et al. 2010, Wang, Bai et al. 2012, Tang, Liu et al. 2016, Luo, Duan et al. 2017, Song, Qi et al. 2017, Lebogang, Bosigo et al. 2019, Yu, Yao et al. 2020). Fig 2.4, shows the schematic diagram of the heterojunction of Co_3O_4 and Ag-loaded Ag_3PO_4. As indicated in this Fig 2.4, the photo-excited electrons and holes transferred to Ag^o and Co_3O_4 respectively. As a result, there is no recombination of holes-electrons and photo corrosion because both carries are no more in or on the Ag_3PO_4 after photoexcitation has been done(Tang, Liu et al. 2016).

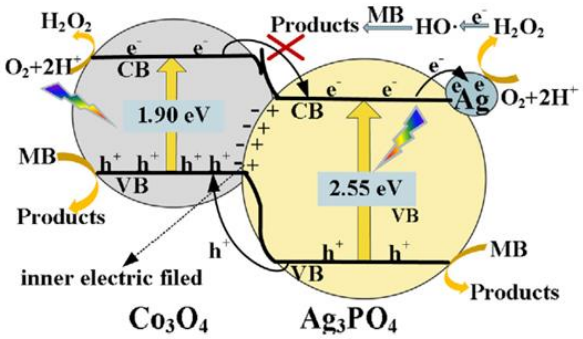

Figure: 2.7.Electrons transfer mechanism in heterostructure photocatalyst (Tang, Liu et al. 2016)

Bi and co-workers grow the silver halides on the surface of rhombic dodecahedral Ag_3PO_4 by the ion change method(Amornpitoksuk and Suwanboon 2014). The valance band and conduction band of all halides are less than Ag_3PO_4 except Cl(Guo, Shi et al. 2018) so that the separation of charge carriers increases, so the recombination rate may significantly be reduced. The summary of reported works on Ag_3PO_4/semiconductor or supporting materials for dye degradation is listed in Table 2.2.

Table:2.2. Summary of reported Ag_3PO_4/semiconductor or supporting materials for dyes degradation

Ag_3PO_4 /SEM.	Types of dyes	Efficiency (%)	References
Ag_3PO_4/CuO	RhB	100% (75 min)	(Yulizar, Bakri et al. 2018)
Ag_3PO_4/ZnO	MB	98.16%(30min)	(Yu, Yao et al. 2020)
Ag_3PO_4/cellulose	MO	90% (80min)	(Lebogang, Bosigo et al. 2019)
Ag_3PO_4/graphen	MB	90% (20min)	(Xiang, Lang et al. 2015)
Paly./Ag_3PO_4	MB	97% (12min)	(Luo, Duan et al. 2017)
Ag_3PO_4/TNS	RhB	99.11%(5min)	(Wang, Li et al. 2017)
Co_3O_4 /Ag_3PO_4	MB	100%(12min)	(Tang, Liu et al. 2016)
Ag_3PO_4/Fe_3O_4	RhB	100% (50min)	(Jun, Kim et al. 2020)
Carbon /Ag_3PO_4	MB	100%(70min)	(Zhu, Zhao et al. 2017)
g-C_3N_4/Ag_3PO_4	MB	96%(10min)	(Zhang, Lv et al. 2017)

2.1.2.1.3. External factor affected Photocatalysis for degradation of dyes

The external factor such as pH of solutions, initially organic(dyes)pollutant concentration, a dose of catalyst, the surface area of catalyst, shape, and size of catalyst, the light of intensity (Rajeshwar, Osugi et al. 2008, Rehman, Ullah et al. 2009).

It was confirmed that a large surface area is favored since the incident UV light can interact with more ZnO surfaces. For instance, the ZnO plates sintered at 700^{o}C was decolorization efficiency in solution was found to be about 95% for Rhodamine red (RR) 180 and 88% for Rhodamine orange-16(RO 16) in 90min. On the other hand, the efficiencies of the plates sintered at 1050◦C reached only 8% for RR 180 and 10% for RO 16 for the same reaction time the efficiency difference for dye degradation due to the surface area of ZnO plates sintered at 700^{o}C has higher surface area than ZnO plates sintered at 1050^{o}C(Yassıtepe, Yatmaz et al. 2008).

The dye degradation efficiency of the catalyst depends on the pH values of wastewater that means at low pH values the surface of the catalyst protonates and becomes positively charged. As result, it is effective for the degradation of negative organic dyes, and at high pH values, the surface of the photocatalyst becomes negatively charged. Hence, it is effective for degradation positive dyes because of strong electrostatic attraction between a negatively charged catalyst and cations dyes. For example, the Photodegradation of Methyl Red is found maximum

at 5 pH because the methyl Red is the cationic dye. The photodegradation of EBT is found maximum at pH =2 because it is an anionic dye that adsorbs maximum at pH=2 value (Kumar and Pandey 2017).

The effect of catalyst dose, the catalyst mount affect the photocatalytic efficiency, at low catalyst loading the photocatalytic degradation efficiency of organic pollutant is low due to the catalyst surface and absorption of light by the catalyst surface are limiting and the active site available at low loading is small and increasing catalyst load is increasing the number of photogenerated electrons. As result, the photocatalytic efficiency increasing parallel with catalyst dose till maximum concentration for optimum activity achieved. However, if the catalyst dose beyond the maximum concentration, the photocatalytic activity decreased due to the irradiation field inside the reaction medium is reduced due to the light scattering by the aggregation of catalyst particles (Akyol, Yatmaz et al. 2004, Coleman, Vimonses et al. 2007, Al Kausor and Chakrabortty 2020).

A dye concentration affects the efficiency of photocatalyst that degradation of organic dyes from wastewater. For instance, Mehdi Al Kausar et al reported that at a higher concentration of AB 25, the ratio of dye particles to the activated sites of NTS@GO (0.6) increases which prevents adsorption of more dye particles onto the surface active sites and consequently the degradation efficiency gradually decreases, so during photodegradation of organic dyes from wastewater initially concentration of the dyes must be under consideration due to the photodegradation efficiency depends on initially dyes concentration. Generally, the photodegradation efficiency of dyes decreased when the dye concentration is increasing(Reza, Kurny et al. 2015).

The effect of reaction temperature, an increase of reaction temperature generally resulted in increasing in photocatalytic activity till the optimum photocatalytic activity is achieved, further increasing of reaction temperature leads to the increase of electron-hole recombination. At high temperatures, and the photodegradation of organic dyes is high due to the high adsorption of dyes on the surface catalyst. Hence, the adsorption of dyes enhances the photodegradation of dyes from wastewater(Mamba, Mamo et al. 2014).

Both light intensity and irradiation time affect dye degradation from wastewater. At low light intensity the photodegradation organic pollutant inside wastewater low but increases

linearly with light intensity. However, at the high light intensity the photodegradation of dyes low due to the competition of photogenerated electron-hole pairs separation and the recombination electron-hole pairs, but at the low light intensity, the recombination electrons–holes pairs is negligible (Asahi, Morikawa et al. 2001, Kundu, Pal et al. 2005). As irradiation time increasing, the formation of reactive oxygen species that mineralizing organic pollutant from wastewater increase linearly this resulted in the photodegradation efficiency is promoted (Gaya and Abdullah 2008).

To the best of our knowledge, there was no report on the synthesis of $Zn_{1-x}Cu_xO/Ag_3PO_4$ composite by in situ precipitation techniques where x=0.005, 0.01, 0.02, 0.03, 0.04. In this work, the property of ZnO was improved by doping Cu metal ions to extend the absorption of solar light into a longer wavelength. The experimental results revealed that the photocatalytic activities of the 5(CZ-1)/A composite were 94% and the degradation rate was 0.0284 min^{-1} which better than that of CZ-1 and Ag_3PO_4. Therefore, the Cu doped ZnO/Ag_3PO_4 composite is a promising material for the degradation of organic dyes from wastewater in practical application.

CHAPTER THREE

3. MATERIALS AND METHODS

3.1.Materials and chemicals

Chemicals :-Zinc nitrate hexahydrate (Zn $(NO_3)_2.6H_2O$) (Loba Chem, 99%,) and copper nitrate tri-hydrate (Cu $(NO_3)_2.3H_2O$) (Sigma Aldrich, 99%) are used as a precursor for synthesizing ZnO and Cu doped ZnO respectively. Potassium hydroxide (NaOH) is used as a precipitating agent ZnO and Cu doped ZnO.$AgNO_3$ (Loba Chem, 99%) and Na_2HPO_4 were used for synthesizing Ag_3PO_4 (silver orthophosphate). Na_2HPO_4 (Sigma Aldrich, 99%) is used as a precipitating agent for preparing Ag_3PO_4. Distilled water and ethanol were also used during the experimental work. Model dye such as methylene blue ($C_{16}H_{18}CIN_3SxH_2O$) was used for the photocatalytic test.

3.2. Methods

3.2.1. Synthesis of Ag_3PO_4

Silver phosphate (Ag_3PO_4) was synthesized by the co-precipitation method at room temperature. According to Pengyu D et al(Dong, Hou et al. 2016) .Firstly, 5.809 g (0.034 mol) of silver nitrate ($AgNO_3$) was dissolved in 40 mL of distilled water. Then, the stoichiometric amount of 1.6183 g (0.01139 mol) of Na_2HPO_4 dissolved in 40 mL of distilled water in the ratio (3:1) $AgNO_3$ to Na_2HPO_4. After that, silver nitrate solution was added drop by drop into Na_2HPO_4 solution under continuous stirring, and immediately the solution changed from white to yellow and further stirring for 30 min to obtain more silver phosphate precipitation. Then, aging overnight at ambient temperature and filtered by centrifuge speed at 2000 rpm for 15 min and can be washed with distilled water severally times. Finally, the silver phosphate was dried in the oven at 100 °C overnight and calcined at temperature 200 ^oC, 300 °C, 400 °C, 500 °C, 600 °C for 2 hr.

3.2.2. Synthesis of $Zn_{1-x}Cu_x$ O

Cu doped ZnO were synthesized from their respective precursors as following. First, 0.5(1-x) M of Zinc nitrate hex-hydrate Zn $(NO_3)_2.6H_2O$ and x(0.5) M of copper nitrate tri-hydrate $Cu(NO_3)_2.3H_2O$ was prepared in a separate bakers by dissolved in the 40 mL of distilled water then, the second solution was added to the first solution to prepare (0.5%, 1%,2%,3%,4%,)

of copper doped zinc oxide, and stirring for 30 min. After that, under continuous stirring a 0.75 M of NaOH was prepared by dissolving in the 80 mL and it was added to the above solution drop by drop until the pH of the solution reached 9.08 to precipitate Cu doped ZnO suspension gel. As result, the color of the solution changed from white to cyan(blue). Then, aging at room temperature for 48 hr. Finally, the solution was filtered by a centrifuge machine and washed with distilled water and ethanol several times. In the end, it dried overnight at 100 ° C and calcined at 500 ° C for 2 hr. The same procedure was applied to the synthesis of ZnO by precipitation method without copper nitrate tri-hydrate. The schematic view of the synthesized Cu doped ZnO was displayed in Fig3.1.The synthesized sample represented as follows CZ-0.5, CZ-1, CZ-2, CZ-3, and CZ-4 for 0.5% ,1%,2%,3%,4%,respectively.

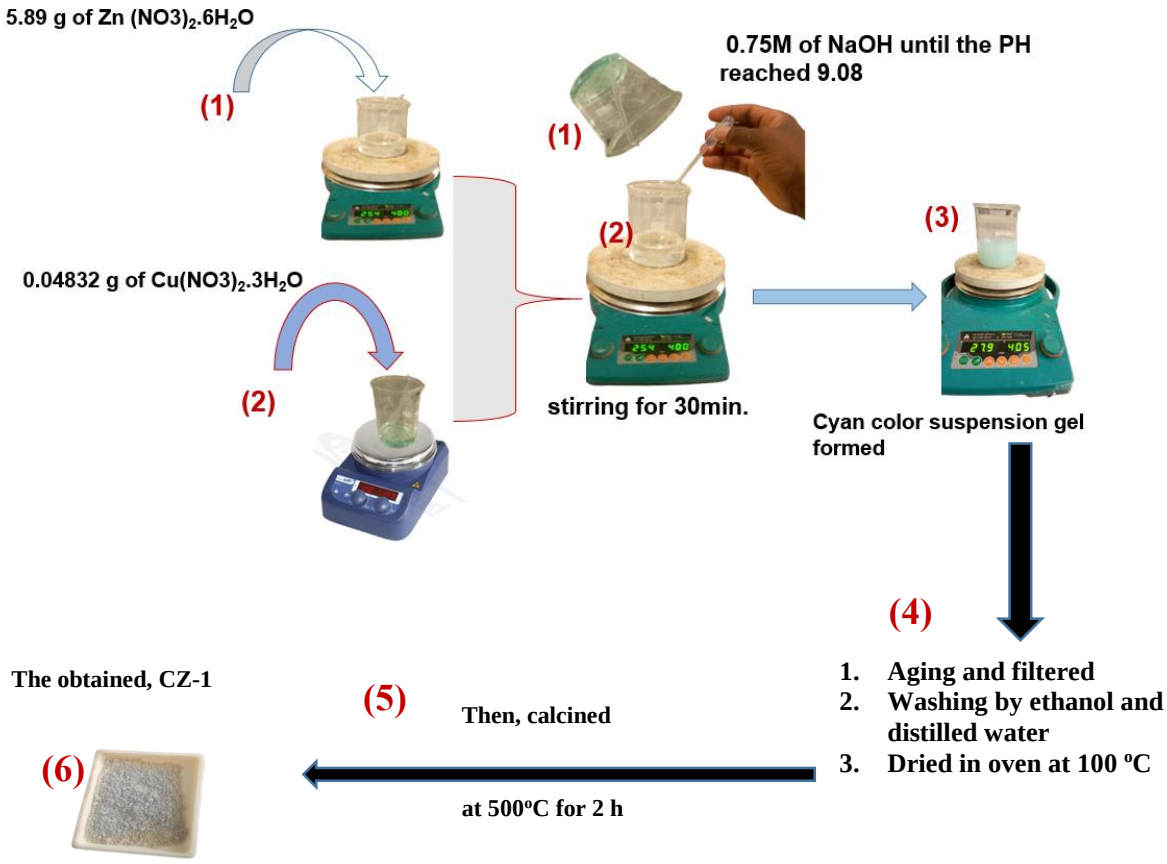

Figure:*3.1 . Schematically diagrams of the synthesizing of CZ-1*

3.2.3. Synthesized of $Zn_{0.99}Cu_{0.01}O)/Ag_3PO_4$ Composite

CZ-1/Ag_3PO_4 in the molar (1:19) ratio were synthesized by in situ precipitation method as follows. First, 0.04881 g (0.0006 mol) of CZ-1 was dissolved in the 40mL of distilled water

and sonicated for 20 min, then 0.5678 g (0.011428 mol) of Na_2HPO_4 adding to the above solution, and stirring for 20 min. After that,5.809 g (0.03384 mol) of $AgNO_3$ dissolved in the 40 mL of distilled water and added to the first solution drop by drop under continuous stirring, followed by stirring for 4 hr and aging overnight then it was filtered and washed by distilled water severally times. Finally, it was dried overnight at 100 ^oC. Schematic diagrams of synthesized Cu doped ZnO/Ag_3PO_4 were depicted in Fig3.2. The synthesis of a 1:39, 1:9 molar ratio of CZ-1 $/Ag_3PO_4$ composite applied the same procedure. The synthesized sample represented as follows symbolically 2.5(CZ-1)/A, 5(CZ-1)/A, and 10(CZ-1)/A.

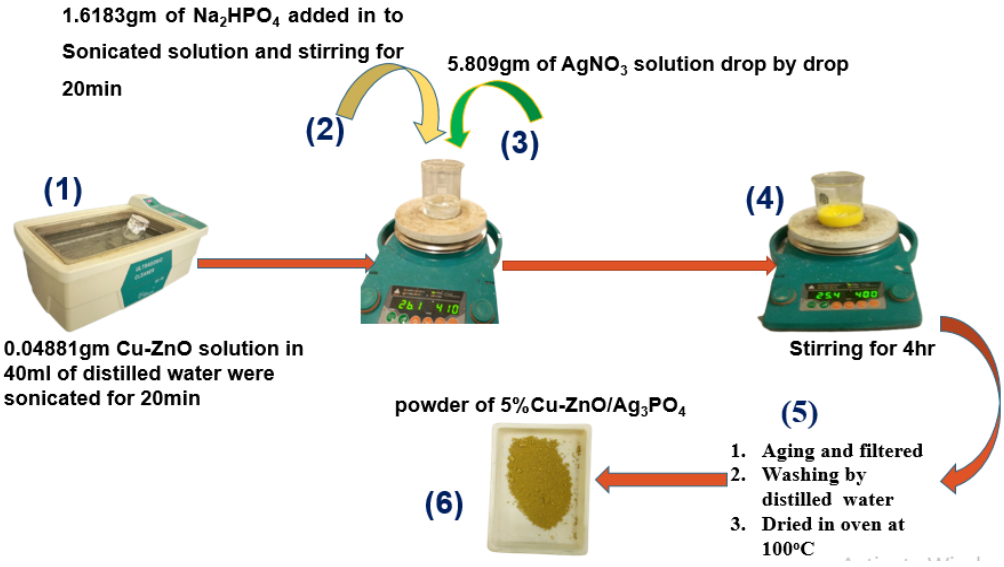

Figure:3.2. Schematically representation Synthesizing of Cu-doped ZnO/Ag_3PO_4

3.2.4. Characterizations

The crystal structure of the synthesized sample was determined by using X-Ray powder diffraction (XRD) (XRD-7000S Shimadzu) equipped with Cu-Kα radiation with wavelength (λ=1.54 Å) operated under a voltage and current of 40 kV and 30 mA, respectively, with wide-angle ranging from 10 ^{o} to 80 ^{o} at a scanning rate of 3 degrees/min. The morphology was studied by using SEM(COXIEM-30). The optical properties of synthesized material such as bandgap, absorption of light, the reflectance were determined by using UV-Visible Diffuse reflectance spectroscopy (UV-visible DRS) (UVvis-3600plus Shimadzu) in the wavelength ranging from 320-800 nm and the bandgap was determined by using barium sulfate ($BaSO_4$) as reference. The

chemical bonding between materials and functional group in a synthesis material was studied by FT-IR spectrometer in the range of 4000-400 cm^{-1} (Ft/IR-6600 type A). The photoluminescence (PL) spectra were studied in the range wavelength from 250nm to 600nm were the excitation wavelength for Cu doped ZnO, Ag_3PO_4, and composite was done at 250nm, and the Xe laser excitation was used for a photoluminescence spectrometer. UV-visible spectroscopy was used for determining the absorbance of dyes lefted inside solution after light irradiated.The thermal property of Ag_3PO_4 was determined using DTA and TGA.

3.2.5. Photocatalytic activity setup

The photocatalytic degradation efficiency of Cu doped ZnO, Ag_3PO_4 calcined at various temperatures, and y(CZ-1)/A (where y=2.5, 5, 10%) composite was determined by the degradation of a methylene blue (model organic dye) from aqueous solution under visible light irradiation (λ>420nm, of 150W halogen lamp). Typically, 0.0222 g of the photocatalyst was added to a 100 mL methylene blue aqueous solution of 10 mg/L, followed by sonication for 40 min to achieve better dispersion and absorption–desorption equilibrium. Then put under the visible light halogen lamp, after that 5 mL of the solution was taken regularly from the reactor at 15 min. The reaction container was supplied with an outside jacket for water circulating to maintain the reaction proceeds at room temperature. Then, the absorbance of the filtered Methylene blue (MB) containing solution at a given time was measured under a UV-visible spectrometer at a wavelength of 664 nm. Finally, the degradation efficiency can be calculated by using equation (3.1)

$$\%\deg radation = 1 - \frac{C_t}{C_o} * 100 \quad \text{.....(3.1)}$$

Where C_o is the initial concentration before adsorption-desorption and C_t is the concentration of the MB at a time *t*.

Then degradation rate constant can be evaluated using the following formula.

$$\ln\left(\frac{C_t}{C_o}\right) = -Kt \quad \text{.....(3.2)}$$

Where *K* is the rate constant, and *t* is the reaction time.

CHAPTER FOUR

4. RESULTS AND DISCUSSIONS

4.1. Thermal analysis For Pristine Ag_3PO_4

The thermal decomposition of a pristine Ag_3PO_4 studied by DTA and TGA is indicated in Fig 4.1(a) and Fig 4.1b (b), the sample was heated in a nitrogen gas atmosphere at a temperature from 0 ^{o} to 1000 ^{0}C. As indicated in the Fig 4.1 (d), the total weight loss of the sample above 400 ^{o}C 1.505 % due to decomposition and melting of Ag_3PO_4. From the DTA in Fig 4.1(a), the endothermic peaks at 522 ^{o}C indicated the melting of Ag_3PO_4. These peaks did not show any phase change in the pristine Ag_3PO_4(Dhanabal, Chithambararaj et al. 2015) (Dong, Hou et al. 2016).Which consistent with the result we obtained in the XRD result in which the normal peaks found in the silver phosphate were starting to remove when calcined at 500 ^{0}C and 600 ^{0}C due to the melting of Ag_3PO_4.

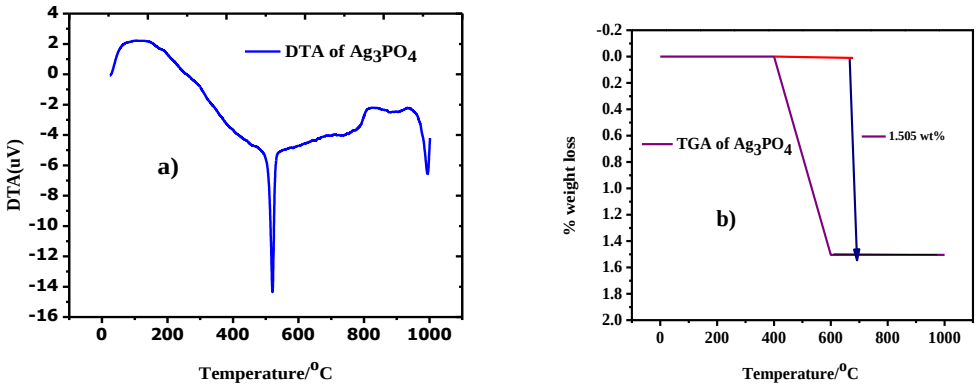

Figure :4.1.a) and b) DTA and TGA for pristine silver phosphate (Ag_3PO_4)

4.2. XRD analysis

Figure 4.2 depicted the XRD patterns of synthesis Ag_3PO_4 dried at 100 °C, and calcined at 200 °C, 300 °C, 400 °C, 500 °C, 600 °C. As shown in Fig.4.2 a, the body-centered cubic (BCC) crystal structure of Ag_3PO_4 of the JCPDS No of 06-0505 have the obvious peaks at 2θ = 20.8°, 29.7°, 33.3°, 36.6°, 42.5°, 47.8°, 52.7°, 55.0°,57.3°, 61.6°, 69.9°, 71.9°, and 73.9°, and the correspondence planes were (110), (200), (210), (211), (220), (310), (222), (320),(321), (400), (420) and (421). From Fig.4.2 a, we observed that a body-centered cubic (BCC) phase of

Ag_3PO_4 was not changed with calcination at low temperature, but the intense and well-defined diffraction peaks and crystallized Ag_3PO_4 BCC crystal structure were decreased when a calcination temperature increased from 200 ^oC, 300 ^oC. According to reported by A.N. Martín-Gómez et al, Ag_3PO_4 heated above 300 ^oC very small new phase such as Ag_2O and Ag^+ nanoparticle metals were detected (Martín-Gómez, Navío et al. 2020).but in our case the pristine Ag_3PO_4 crystal structure retained its peaks and showed good thermal stability till the calcination temperature reached 400 ^oC this might be due to lack of instrument to detected Ag_2O and Ag^+. Beyond this, the temperature at 500 ^oC and 600 ^oC lost its structure and crystallinity. A As indicated in Fig 4.1 b the XRD result for 200 ^oC and 600 ^oC used for comparing .As result , some of the peaks found in the pristine Ag_3PO_4 may hide or missing from the respective peak Ag_3PO_4 calcined at temperature of 600 ^oC when compared to the one calcined at 200 ^oC this due to change in phase, or melting of Ag_3PO_4 and it would be owing to changing from polycrystalline to single crystal.As we knew in another material, calcination at high temperature improved crystallinity(Noda, Lee et al. 2008). However, in the case of Ag_3PO_4, the relative intensity of the main peak (210) concerning the intensity diffraction peak (211) was decreased as calcination temperature increased, meaning that the crystallinity of these materials slightly decreased due to it lost its structure and orderity of atoms by melting at high temperature. Our result disproved the idea suggested by Ruifeng. C et al (Chong, Cheng et al. 2016), but consistent with the result reported by martin G et al (Martín-Gómez, Navío et al. 2020).

Table: 4.1. Determination of average crystalline size (D) (nm), FWHM (β°), Shifting of 2θ angle, changing of interplanar distance (d) (Å) for the Ag_3PO_4 calcined at various temperatures.

Sample	**2θ(°)**	**FWHM(β°)**	**d(Å)**	**Av. Crystalline size(D)(nm)**	**Micro-strain(ε)(10^{-3})**
100 ºC-Ag_3PO_4	33.4005	0.1605	2.68057	47.40632	0.670775
200 ºC-Ag_3PO_4	33.3847	0.1636	2.6818	46.50996	0.683759
300 ºC-Ag_3PO_4	33.3037	0.2167	2.68814	35.12063	0.90588
400 ºC-Ag_3PO_4	33.3522	0.1504	2.68434	50.59625	0.628644
500 ºC-Ag_3PO_4	33.33	0.1501	2.68607	50.70032	0.627426
600 ºC-Ag_3PO_4	33.2396	0.096	2.69317	79.29076	0.40138

As listed in Table 4.1, The calculated average crystalline size of silver phosphate dried at 100 ºC and calcined at T=, 200 ºC, 300 ºC, 400 ºC, 500 ºC, 600 ºC by using the Scherrer formula in equation 4.1, the results revealed the increase a calcination temperature from 200 ºC to 300 ºC, decreasing of crystalline size from 46.5099nm to 35.12063nm owing to broadening of diffraction angle FWHM (β) and increasing of the micro-strain which prevented nucleation and crystalline growth. However, further increasing of calcination temperaturefrom 300 ºC to 400 ºC, 500 ºC, 600 ºC) increasesthe crystalline size which due to fusion or sintering, and melting of Ag_3PO_4 to form large size by aggregated, and diffusion particle to each other, and this contributed to lowering micro-strain at high temperature or releasing of a strain which causes for enlarged crystalline size.

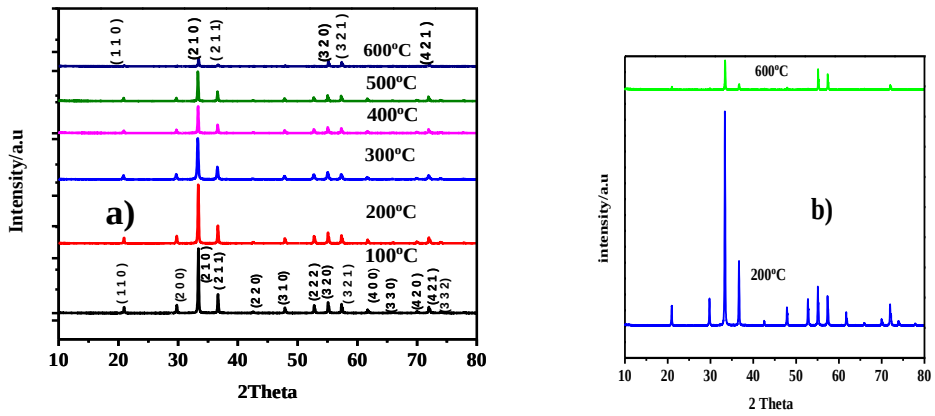

Figure :4.2a) XRD result of Ag_3PO_4 dried at 100 ^oC, and calcined at 200 ^oC, 300 ^oC, 400 ^oC, 500 ^oC, 600 ^oC b) XRD result of Ag_3PO_4-200 ^oC and Ag_3PO_4-600 ^oC

Figure 4.3a ,shows the XRD result of ZnO and ($Zn_{1-x}Cu_xO$) powders where (x=0.005, 0.01, 0.02, 0.03, 0.04). It revealed that the higher intensity peaks of the planes (101) along with (100), (002), (102), (110), (103), (200), (112), (201), and (202) planes found in a pristine ZnO and for all Cu doping ZnO. All the diffraction patterns corresponding to the wurtzite crystal structure of ZnO of the space group P63mC (186) with the reference code of [JCPDS.No-00-036-1451]. The evidence from the XRD result there are no additional peaks emerged related to Cu, and CuO for small doping of the Cu due to copper ions (Cu^{+2}) was replaced Zn^{+2} ions lattice site rather than the occupied interstitial site. However, as the concentration of Cu increase the new phase has emerged between 42° and 43° which was corresponding to the (111) plane of CuO [matched with JCPDS data card No .05-066]. The CuO formed when access Cu^{2+} ions left in the system solution reacted with oxygen.

The replacement of Cu^{+2} ions for Zn^{2+} ions in the lattice site of ZnO affects the concentration of the interstitial Zn, oxygen vacancies, Zn vacancies(Muthukumaran and Gopalakrishnan 2012). From, Fig 4.3 a, we revealed that the intensity of all planes decreasing as the concentration of Cu in the ZnO lattice increasing, the reducing of intensity owing to the defect and disorder formed by incorporation of Cu^{+2} ions into the ZnO crystal structure (Kadam, Kim et al. 2017). There was a small shift diffraction angle toward a large angle due to shrinkage of the ZnO lattice by incorporation of a small tetrahedral ionic radius of Cu^{+2} ions in the ZnO lattice site when compared to Zn^{+2} ions(Iribarren, Hernández-Rodríguez et al. 2014).However ,Cu^{+2} ionic radii (0.072 nm) ,and Zn^{+2}(0.074 nm) are very close to each other ,that is why $Cu^{+}2$

easily substituted to ZnO lattice site , (Kadam, Kim et al. 2017). As indicated in the follows Fig 4.3 b for x=0.005 the diffraction angle shifted to a large angle which is (Δ2θ=0.03087) in the strong peaks (101) due to substitution small ionic radius of Cu^{+2} (0.072 nm) ions in the lattice site of ZnO for Zn^{+2}(0.074 nm) ions. However, for CZ-1, CZ-2, CZ-3, and CZ-4 the 2θ shifted toward a small angle by the Δ2θ=(-0.02743, -0.04163, -0.02443, -0.02203), respectively owing to substitute a large tetrahedral ionic radius of Cu^{+} into ZnO lattice site. The electronegativity of Zn and Cu metals play prominent roles in the reactivity of Cu metals in the ZnO lattice site. It is known that as electronegativity decreases, the reactivity will increase, so the electronegativity of Zn and Cu could be 1.65 Pauling and 1.9 Pauling, respectively. So Zn needs less ionization energy to loss electron and its become higher reactive than Cu metal (Allred 1961, Asrofi, Abral et al. 2017). The average crystalline size of ZnO and Cu doped ZnO was determined by Scherer's formula by using existing XRD data and assuming crystalline were cubic monodisperse in a size. All given data of XRD have been by fitting with a gaussian distribution function.

$$D = \frac{K\lambda}{\beta \cos\theta} \quad \text{.....4.1}$$

Where D is the average crystalline size(nm),β°(FWHM) is the full-width half-maximum,λ(0.1504nm) is the wavelength of X-ray radiation, K(0.94) is Scherer's constants.

The result clearly showed that the average crystalline size decreasing from 32 nm to 25.8 nm for the Cu doping ZnO (when x=increased from 0 to 0.005) and (when x=0, 0.01, 0.02 0.03) the average crystalline size decreasing from 32 nm to 15 nm whereas for x=0.04 the crystalline raised to 20.67 nm . The decreasing of crystalline size due to the shrinkage, and distortion of the ZnO lattice site by external impurity inhibited nucleation and crystal growth of ZnO consequently, the particle size becomes smaller (Ashokkumar and Muthukumaran 2015). The FWHM shows the inverse trend of the crystalline size which matched with the relationship in the Scherer equations, the FWHM value listed in Table 4.2, For the $Zn_{1-x}C_xO$ (where x is from 0.005 to 0.04). and the larger crystalline size and small value of FWHM for CZ-4 than CZ-3 due to the combined effect of copper ions substituted Zn^{2+} ions lattice site and the formation of the more secondary phase of the copper. Residual strain (ε) increasing with increasing Cu

contents and causes for decreasing of crystalline size and it was calculated by the following equation 4.2 (Ashokkumar and Muthukumaran 2015).

$$\varepsilon = \frac{\beta \cos\theta}{4} \quad \text{.....4.2}$$

Where ε is the residual micro-strain

Table: 4.2. The 2θ(°), FWHM(β°),d-value(Å) ,the change diffraction angle (Δ2θ(Å) ,average crystalline size(D) ,micro-strain(ε) of Pristine ZnO and Cu doped ZnO.

Sample	2θ(°°)	FWHM(β°°)	d-value(Å)	Δ2θ(°)	Av .crystalline size (D)(nm)	ε(micro-strain)*10^{-3}
ZnO	36.33453	0.2358	2.46985	0	32.0092408	0.978
CZ-0.5	36.3654	0.2924	2.46853	0.03087	25.81091476	1.212129
C Z-1	36.3071	0.2592	2.47236	0.02743	29.12180418	1.074679
CZ-2	36.2929	0.2747	2.47329	0.04163	27.47971708	1.138991
CZ-3	36.3101	0.479	2.47282	0.02443	15.7584694	1.985983
CZ-4	36.3125	0.3651	2.472	0.02203	20.67448645	1.513732

According to a working principle of XRD. The interplanar spacing (‘d’)and the diffraction angle was related by Bragg's law in equation 4.3.

$$n\lambda = 2d\sin\theta \quad \text{.....4.3}$$

Where n=1,2,3…….**λ** is the wavelength of the incident X-ray beams

At the lower copper concentration of x=0.005 the d spacing decreasing due to shrinkage of lattice site),by substitution of small Cu^{+2} ions instead of Zn^{+2} ions. As result, a diffraction angle

was shifted to a larger angle (Liu, Yang et al. 2009). The same result was reported by Kuylk et al(Kulyk, Sahraoui et al. 2009).Although increasing of the inter-planar distance(d) for Cu doping ZnO (x=0.01,0.02,0.03,0.04) compared to ZnO because of substitution large radius Cu^{+} ions for Zn^{+2} ions.Consequently, their diffraction angles were shifted to small angles. The same trend was reported by S. Muthakumaran et al(Liu, Yang et al. 2009, Muthukumaran and Gopalakrishnan 2012). We concluded that, for x= 0.005 small ionic radius Cu^{+2} ions substituted for Zn^{+2} ions whereas for (x=0.01, 0.02, 0.03, 0.04) larger ionic radius of Cu^{+} ions was repaced for Zn^{+2} ions,and slight shift of diffraction angles and change interplanar distance(d) indicated that a Cu really doped in to ZnO lattice site.

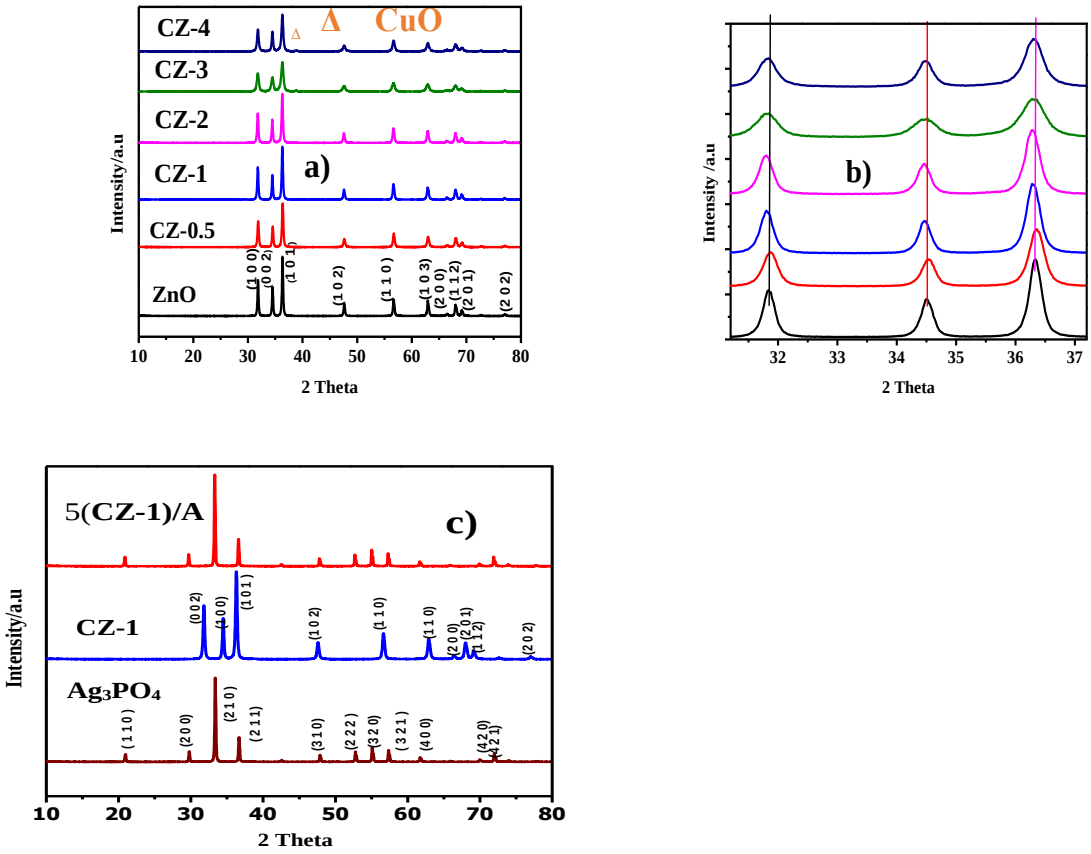

Figure:4.3.a) XRD result of pristine ZnO and $Zn_{1-x}Cu_xO$ (where x=0, 0.005, 0.01, 0.02, 0.03, and 0.004),b) XRD result showed shifting of angle by doping c) XRD result of Ag_3PO_4, CZ-1, and 5(CZ-1)/A composite.

Figure 4.3c shows that the XRD result of a single component such as Ag_3PO_4-100 ^oC, CZ-1, and the XRD result of the 5(CZ-1)/A composite. As indicated in Fig4.3c, for the5(CZ-

1)/A composite all peaks corresponding to 2θ=20.8 °, 29.7 °, 33.3 °, 36.6 °, 42.5 °, 47.8 °, 52.7 °, 55.0 °,57.3 °, 61.6 °, 69.9 , 71.9° , and 73.9 °, and the correspondence planes was (110), (200), (210), (211), (220), (310), (222), (320),(321), (400), (420) and (421) so that all peaks have seen the same to a pristine silver phosphate of dried at 100 ºC(Ag_3PO_4 -100 ºC) of the body-centered cubic crystal structure (BCC) with a JCPDS No of 06-0505. The peaks of CZ-1 did not detect in the composite due to its smallest amount

4.3. SEM analysis

Figure 4.4, indicated the morphology of synthesized samples, (a, b) for Ag_3PO_4 (c, d) for CZ-1 (e, f) for 5(CZ-1)/A. As shown in a fig4.4(a,b), Ag_3PO_4 has a spherical shape morphology with large particle size.Fig4.4(c,d), shows the morphology of a 1% Cu doped ZnO (CZ-1) and it has a spherical-like shape with a small size. Moreover, as shown in Fig 4.4(e,f), the morphology of 5(CZ-1)/A composite similar to Ag_3PO_4, but the small spherical particle size of CZ-1 dispersed on the surface of Ag_3PO_4 which offers a high surface area for the composite. Therefore, the deposited CZ-1 on the surface of Ag_3PO_4 was observed from the SEM image of the composite, t indicating the formation of Cu doped ZnO/Ag_3PO_4 composite.

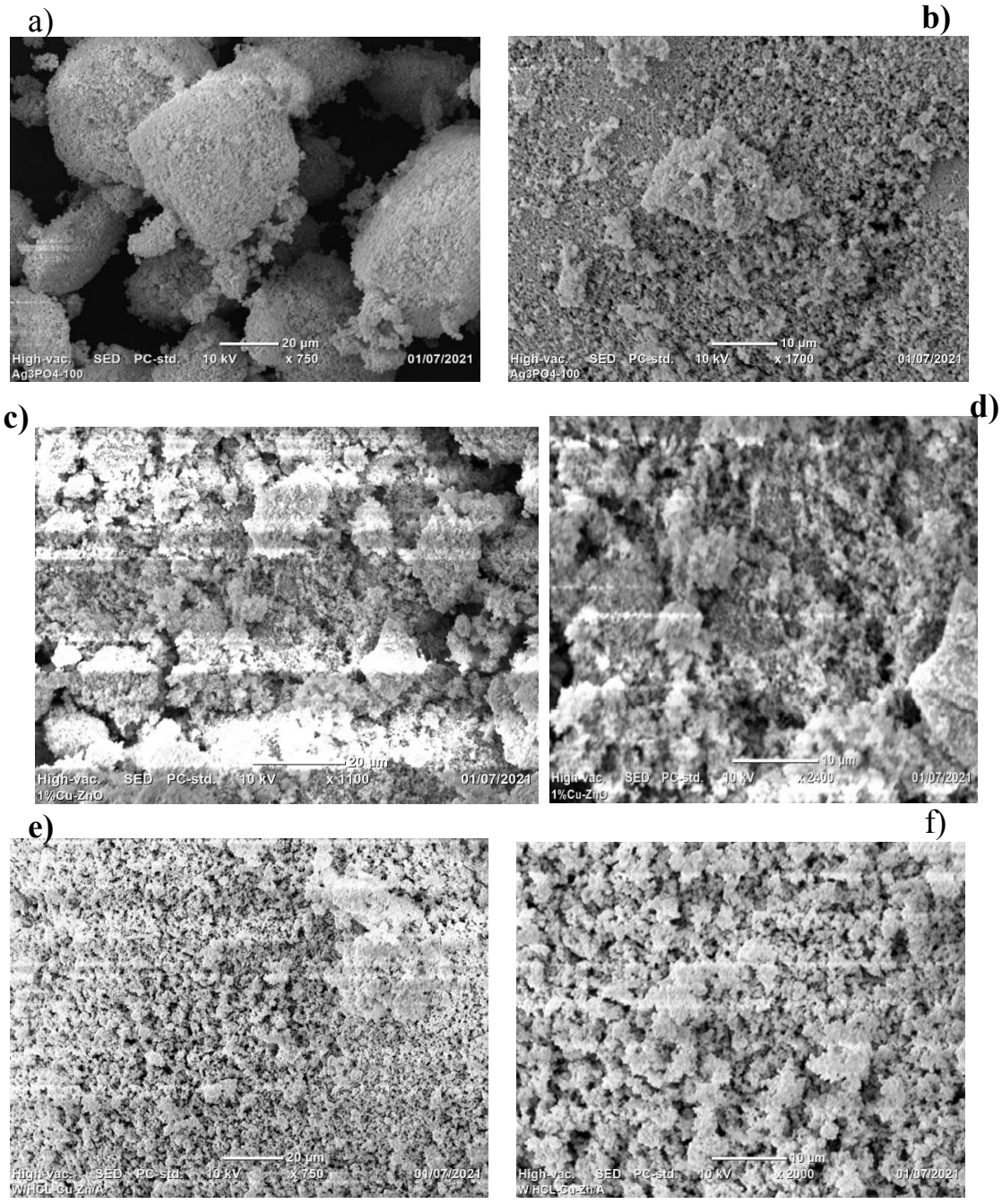

Figure: 4.4 .SEM image of a) and b) for Ag_3PO_4 ,c) and d) for CZ-1,e) and f) for 5(CZ-1)/A

4.4. UV-Visible absorbance study

Figure 4.5(a) indicated UV-vis DRS absorption spectra of Ag_3PO_4 dried at 100 ºC, and calcined at 200 ºC, 300 ºC, 400 ºC, as shown in Fig 4.5(a), absorption of Ag_3PO_4 calcined at 200 ºC high in both UV–region and a visible region, and the absorption edge for 200 ºC was about 533 nm L et al (Luo, Xu et al. 2015).All silver phosphate harvest visible light, but the percentage harvest light i dependi on the bandgap of Ag_3PO_4, thus among Ag_3PO_4 dried at temperature 100 ^{0}C, and calcined at 200,300,400 ^{0}C, the one calcined at 200 ºC have high absorption of light when because silver nanoparticle decorated on the surface of Ag_3PO_4 when it calcined at high temperature helping to harvest large solar light due to it have plasmon resonance effect, thus the absorption of Ag_3PO_4-200 ^{0}C in UV region and visible region high . Fig 4.5 (c, d, e, f), shows the bandgap determined by using the Kubelka-Munk function(Chandekar, Shkir et al. 2020).

$$\boldsymbol{F(R)} = \frac{\boldsymbol{K}}{\boldsymbol{S}} = \frac{\boldsymbol{(1-R)^2}}{\boldsymbol{2R}} \quad \text{4.4}$$

Whereas, F(R) Kubelka-Munk function, k absorption coefficient, s is the scattering factor), R is reflectance.(Banu Bahşi and Oral 2007).

The bandgap (Eg) determined from the following relations.

$$(\boldsymbol{F(R)h\nu})^{\frac{1}{n}} = \boldsymbol{A(h\nu - Eg)} \quad \text{4.5}$$

Where n=1/2 for direct bandgap semiconductor and n=2 for indirect semiconductor (Taddesse, Alemu et al. 2020).As reveals in Figure 4.5. (c,d, e, f), the bandgap of Ag_3PO_4-100 ^{0}C, Ag_3PO_4-200 ^{0}C, Ag_3PO_4-300 ºC, Ag_3PO_4-400 ºC were 2.47 eV,2.49 eV,2.45 eV,2.44 eV respectively, so it ascribes that calcination of Ag_3PO_4 not have an effect on its band gap . high absorbance of light for Ag_3PO_4 calcined at 200 ºC due to silver nanoparticle decorated on the surface of Ag_3PO_4this happened due to structural modification or shrinkage, and decomposition of Ag_3PO_4 during calcination at high temperatures. This result suggested Ag_3PO_4 calcined at 200 ºC harvesting a large amount of solar light to generate charge carriers which attributed to degrade organic dyes from aqueous solution.

Figure 4.5b. Reflectance versus wavelength, as we have seen from Fig 4.5b , the percentage of reflectance for CZ-1 is low when compared to pure ZnO in the visible region this

shows doping causes little shrink a bandgap of ZnO which was attributed to the redshift of the absorption edge ZnO to a longer wavelength. Red-shifted recognized (improved) the incorporation of Cu into the ZnO lattice site. Consequently, the reflected light is low as shown in Fig 4.5b, in the visible light range. The red shifted to a longer wavelength owing to the micro-strain in a ZnO lattice structure which attributed to the decrease optical band gap of ZnO. Incorporation of Cu in the ZnO decreasing the band structure. The small size has a high surface area to volume ratio with a larger optical band gap, but in the case of Cu-doping inverse trends were being observed. The decrease of band gap as we have seen for CZ-1 when compared to ZnO in Fig 4.5g, owing to p-d electron interaction between free electrons in the valance band and localized d-electrons in the metals (Diouri, Lascaray et al. 1985, Li, Li et al. 2011).so the calculated bandgap by using the Kubelka –Munk function in equation (4.4) and by The band gap for CZ-1, and pristine ZnO is 3.24 eV and 3.26eV respectively. Theoretical the bandgap of Cu-doped ZnO was estimated by Vegard laws as follows in equation 4.6.

$$(Zn_{1-x}Cu_xO)=Eg\ (xCuO)+Eg(1-x)ZnO \quad \text{.....4.6}$$

where x is the molar ratio of Cu ions and Eg the bandgap of respective materials(Chandekar, Shkir et al. 2020).

The optical band gap (Eg) of ZnO and CuO is 3.37eV,1.2 eV respectively (Bouras, Mecif et al. 2018).The calculated band gap for CZ-1 is 3.34 eV .so from both experimental and theoretical theory the bandgap of ZnO shrink with the incorporation of Cu ions in the ZnO lattice. Our result was consistent with theoretical and experimental data (Chandekar, Shkir et al. 2020).

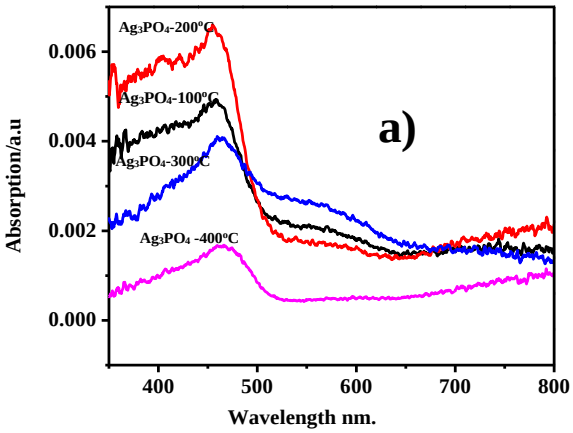
Ag3PO4-200°C
Ag3PO4-100°C
Ag3PO4-300°C
Ag3PO4 -400°C
a)
Absorption/a.u
Wavelength nm.

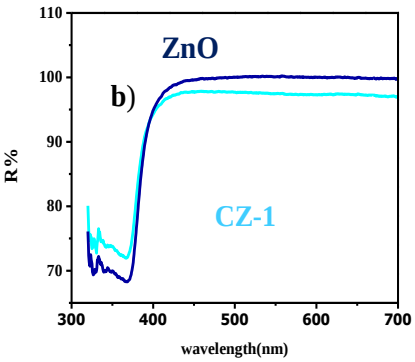
ZnO
b)
CZ-1
R%
wavelength(nm)

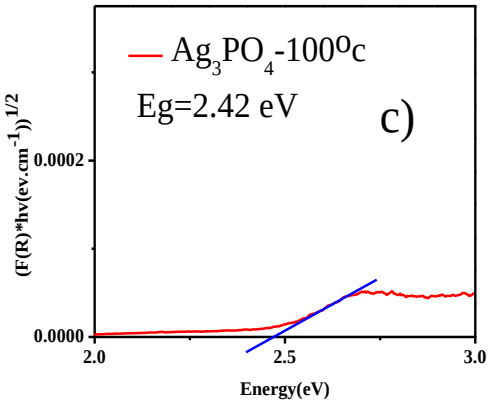
Ag3PO4-100°c
Eg=2.42 eV
c)
(F(R)*hv(ev.cm-1))1/2
Energy(eV)

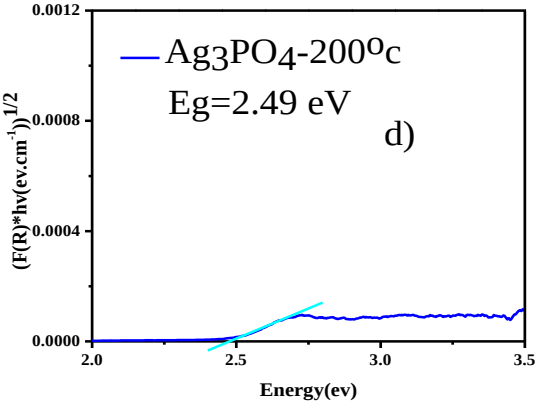
Ag3PO4-200°c
Eg=2.49 eV
d)
(F(R)*hv(ev.cm-1))1/2
Energy(ev)

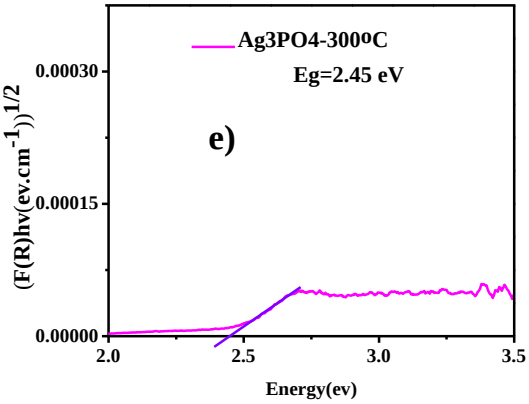
Ag3PO4-300°C
Eg=2.45 eV
e)
(F(R)hv(ev.cm-1))1/2
Energy(ev)

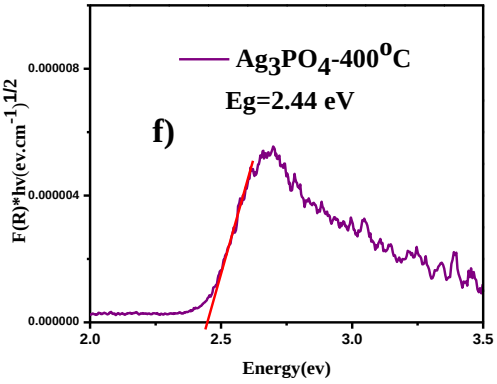
Ag3PO4-400°C
Eg=2.44 eV
f)
F(R)*hv(ev.cm-1)1/2
Energy(ev)

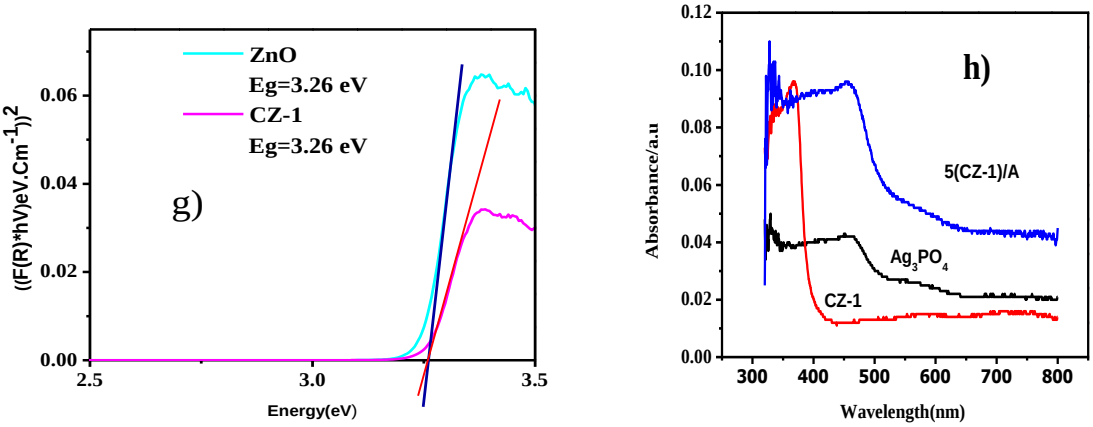

Figure:*4.5.UV-Visible diffuse reflectance spectroscopy(DRS):-a)Absorption for Ag_3PO_4 calcination at various temperature b)%R vs wavelength for ZnO and Cu doping ZnO ,c),d),e),f) the calculated band gap of Ag_3PO_4 dried at 100 °C and calcination at temperature ,200 °,300 °,400 °C respectively)g) Band gap calculation for ZnO and CZ-1 h) Light Absorption of 5(CZ-1)/A ,Ag_3PO_4 ,CZ-1.*

From the UV-Visible diffuse reflectance spectroscopy (DRS). As shown in Fig 4.5(h), the absorption edge of CZ-1 and Ag_3PO_4 was 370 nm, 467 nm respectively. We noted that CZ-1 high absorption in the ultra-violate region than Ag_3PO_4. When CZ-1 was combined with Ag_3PO_4 the absorption edge 456nm which between the absorption edge of CZ-1 and Ag_3PO_4.The absorption ability of the 5(CZ-1)/A composite in the visible range is high when compared to the single component due to the absorption of two materials have been superposed which contributed to enhance the absorption of visible light for composite . .

Photoluminescence spectroscopy (PL) adopted in Fig 4.6(b), to study recombination of photogenerated electron-hole pairs in the composite in detail. In general, the higher photoluminescence peaks indicated high recombination of electron-hole pairs. As shown in Fig 4.6(b), the PL of CZ-1, Ag_3PO_4, and 5(CZ-1)/A excited at a wavelength of 250nm, and the observed intensity for the composite much lower than CZ-1 and Ag_3PO_4 which refers to the recombination photogenerated electron-hole pairs inhibited by the formation heterojunction between CZ-1 and Ag_3PO_4 due to the charge transferring between single component semiconductor interface. Consequently, charge carriers recombination is suppressed which will improve the photocatalytic activity of a single component where the heterojunction is formed

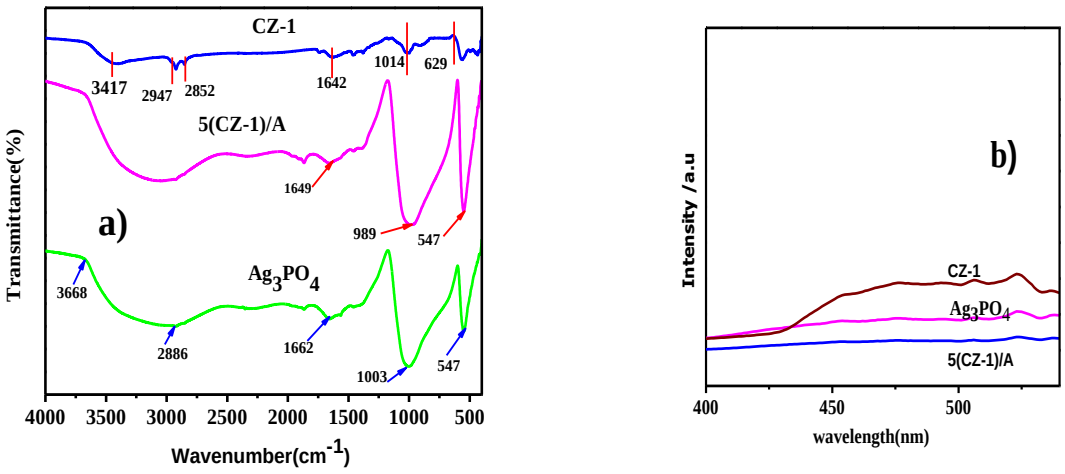

Figure: 4.6.FT-IR spectra of Ag_3PO_4, CZ-1, and 5(CZ-1/A) composite b) The photoluminescence spectroscopy CZ-1, Ag_3PO_4, and (CZ-1/A).

3.5. FT-IR analysis

Figure 4.6(a) Displays FT-IR spectra of Ag_3PO_4, CZ-1, and 5(CZ-1)/A composite. As recognized in the Ag_3PO_4, a wide absorption of spectra in the range of 2886 cm^{-1} to 3668 cm^{-1} ascribe that O-H stretching vibration bond and the peaks at 1662 cm^{-1} O-H-O bending vibration bond due to adsorption of water on the surface of catalyst which can be attributed for adsorption of polar molecules(Zhu, Duan et al. 2020). The two peaks were found at 547 cm^{-1} and 1003 cm^{-1} could be indicated the characteristics of asymmetric stretching of P-O bond and bending vibration of P-O bond of $PO4^{3-}$(Zhu, Duan et al. 2020).

For the pure Cu-ZnO the peaks in the range of 400-600 cm^{-1} corresponding to the Zn-O bond, and the peaks in the range of 629-1014 cm^{-1} belong to the stretching vibration of Cu-Zn-O and change microstructure feature of ZnO, due to the addition of Cu into the Zn-O lattice structure (Muthukumaran and Gopalakrishnan 2012). The broad absorption peaks observed at around 3417 cm^{-1} and 1642 $cm^{-1}$are attributed to the O-H stretching vibration of water (H_2O) in the Cu-Zn-O lattice structure (Muthukumaran and Gopalakrishnan 2012). This may be due to atmospheric moisture or moisture absorbed on the surface of the catalyst and peaks appeared between 2852 cm^{-1} and 2947 cm^{-1}, are attributed to the existence of CO_2 molecules in the air which ascribe the streaching of C-O bond. (Vijayaprasath, Murugan et al. 2015). Moreover, the peaks at 1003 cm^{-1} shifted to 989 cm^{-1} in the 5(CZ-1)/A which ascribed the formation of composite by strong interaction between Cu-ZnO and Ag_3PO_4. However, the actual peaks of a

pure CZ-1 were not be detected on the composite since a small content of CZ-1 exists in the composite(Zhu, Duan et al. 2020).

4.6. Photocatalytic activity Evaluation

Under this section, the photocatalytic activity to degrade methylene blue, for Ag_3PO_4 dried at 100 ºC and calcined at ,200,300,400,500,600 ºC and ZnO,CZ-0.5 ,CZ-1,CZ-2,CZ-3,CZ-4 and for 2.5(CZ-1/A), 5(CZ-1/A), 10(CZ-1)/A composite are discussed in this section.The different external parameters which affected the photocatalyst activity were studied and the photogenerated charge transferring principle for Z scheme CZ/A-5 has been proposed and is discussed under this part.

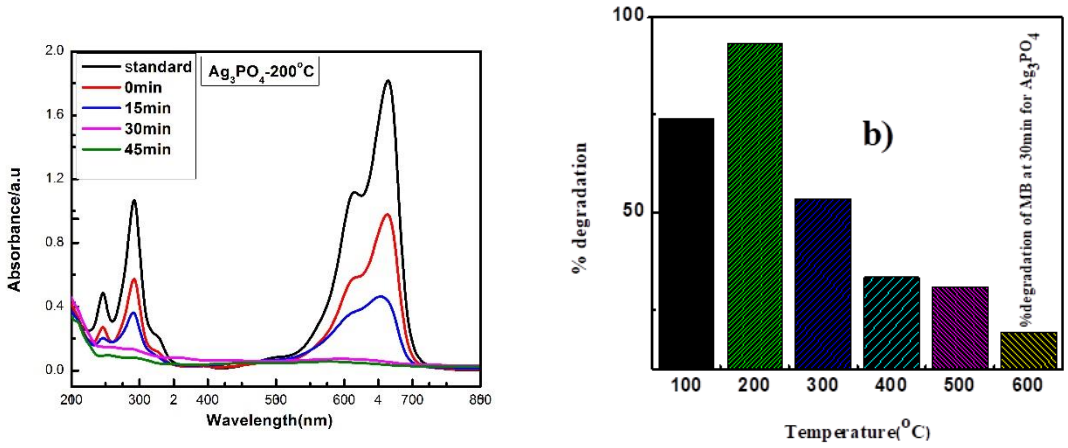

Figure: 4.7.UV-visible spectroscopy absorbance of MB by Ag_3PO_4 at 200 ºC and b) degradation efficiency of Ag_3PO_4 calcined at various temperatures.

The photodegradation efficiency of methylene blue for pristine Ag_3PO_4 and Ag_3PO_4 calcined at different temperatures was elucidated in Fig 4.7, the photodegradation efficiency of Pristine Ag_3PO_4, and Ag_3PO_4 calcined at different temperatures listed in decreasing order as followsT-200 ^{0}C>T-100 ^{0}C>T-300 ^{0}C>T-400 ^{0}C>T-500 ^{0}C>T-600 ^{0}C.Fig 4.7a, indicated the absorbance of methylene blue at various times for Ag_3PO_4 calcined at 200^{o}C, and the absorbance of methylene blue closed to or almost zero when the reaction time reached 30 min. Hence, Ag_3PO_4-200 ^{O}C completely removes MB in 30min.

From Fig 4.7b we were understanding that, the photocatalytic activity Ag_3PO_4 calcined at 200 ºC higher than others which it is degradation efficiency 98% at 30min which matched

with previously reported by Pengyu which the degradation of Ag_3PO_4 calcined at temperature 200 ºC was 96 % 60 min this reveals high photocatalytic efficiency to degrade methylene blue (Dong, Hou et al. 2016). This calcination of Ag_3PO_4 significantly enhanced the photocatalytic activity toward degradation organic dye from aqueous solution due to the formation of oxygen vacancy which enhanced charge mobility and reducing recombination of charge carriers which both are contributed to enhancing photocatalyst activity. Ag^o NPs decorated on the surface of Ag_3PO_4 when it is calcined at 200 ºC enhance the visible light absorption at localized point which matched with the result obtained at Fig 4.5 a . Since Ag^o nanoparticles have localized surface plasmonic resonance (LSPR) effect. In addition to this, silver decorated on the surface of silver orthophosphate inhibited photo corrosion and delayed charge carriers recombination by scavenged the electron in the conduction band before combining with Ag^+ ions in an interstitial site (Li, Fang et al. 2015). However, if the amount of silver decorated on the surface Ag_3PO_4 excess amount its shielding and overshadow the LSPR effect has been occurred and undermining the photocatalytic activity Ag_3PO_4. Therefore, the degradation efficiency of Ag_3PO_4 was calcined at 300 ºC and 400 ºC low compared to others.

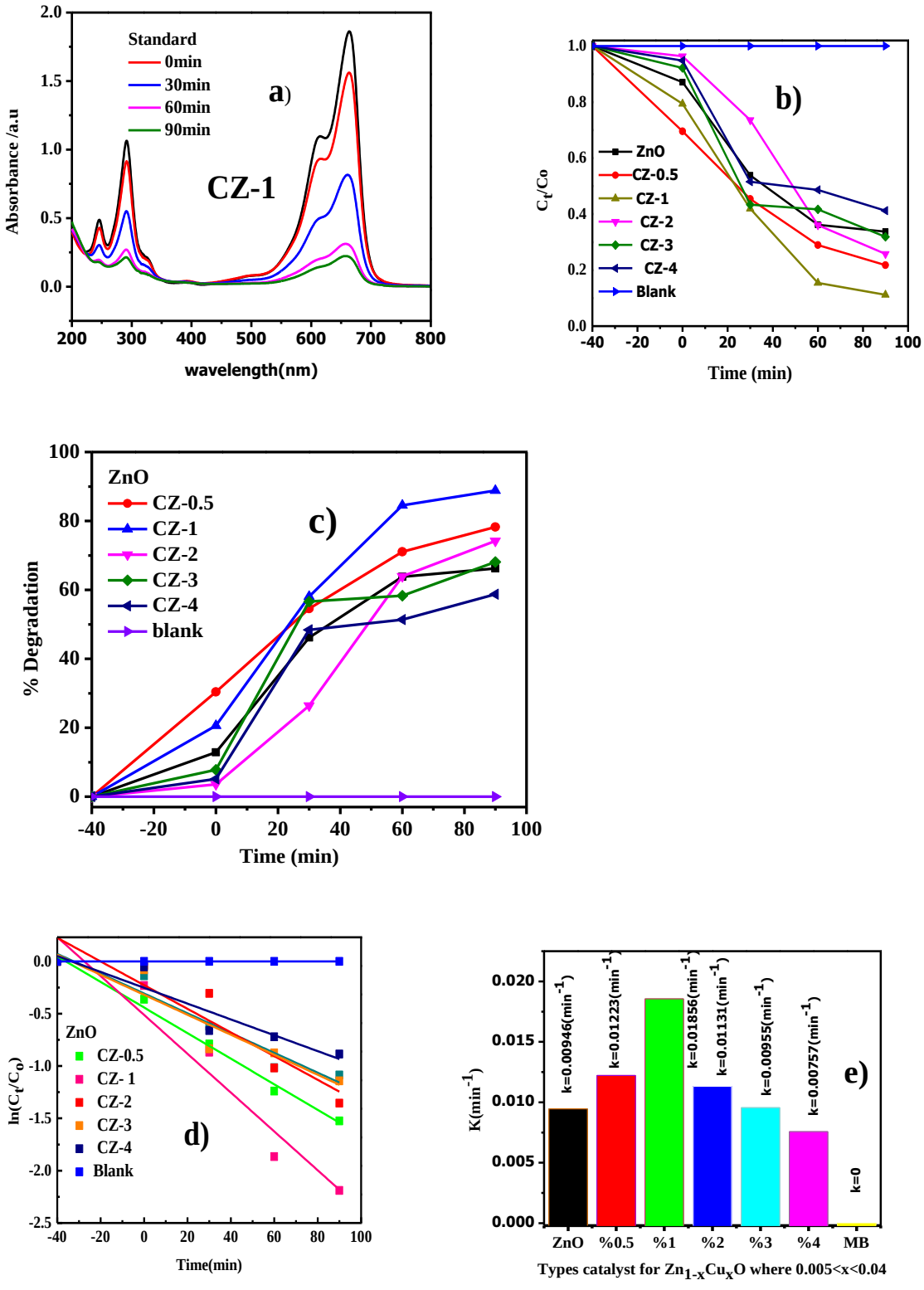

Figure :4.8.The photo-degradation efficiency of $Cu_xZ_{1-x}O$(where x=0 to 0.04).a) Absorbance of MB vs wave length at various time b) C_t/C_o vs time c)% degradation Vs time d) $Ln(C_t/C_o)$ Vs time e) determined rate constant for Cu doping ZnO and pristine ZnO (K)(min^{-1}).

Figure 4.8 showed that the photocatalytic activity of pristine ZnO and Cu doping ZnO when the doping molar percentage of Cu was 0.5%,1 %,2 %,3 %,4 %. The photocatalytic activity depending on the amount of impurity or Copper inside pristine ZnO, the photocatalytic performance of the pure ZnO and Cu doping ZnO was evaluated toward degradation of methylene blue(MB) under visible light..

From Fig 4.8 b, we observed that the degradation of the dye from the aqueous solution increasing with increasing the content of Cu^{+2} from 0.5 % up to 1 % and then further increasing of the Cu^{+2} ions content decreasing degradation efficiency of the dyes, so a CZ-1 has high photodegradation performance than pure and others doped ZnO. Fig 4.8a shows that the decrease of the absorbance of methylene blue (MB) as time photo reaction increasing for CZ-1, and reached minimum value at 90min. Fig 4.8b, indicated C_t/C_o versus photoreaction time to degrade the dyes by ZnO and Cu doped ZnO, so from the result we have seen that CZ-1 highly reducing the initial concentration of the dyes at 90min.Fig 4.8d, shows that degradation efficiency of pristine ZnO and Cu doping doping ZnO from the result we observed that the degradation efficiency to remove methylene blue (MB) for a pristine ZnO ,CZ-1,CZ-2,CZ-3 and CZ-4 was 66 % ,78% ,88% ,74% ,68 % ,58 % respectively. Fig 4.8d, shows that the ln (C_t/C_o) versus photoreaction time for degradation of dyes from aqueous solution. From the result we were understanding ln (C_t/C_o) decreasing linearly as the time of the photoreaction was increasing. Linearly relationship explains that the degradation of methylene blue (MB) from aqueous solution is following pseudo-first-order kinetics given by the above equation 3.2. From the plot of ln (C_t/C_o) versus reaction time, the rate constant was calculated as slope and it was listed in Fig 4.8e, for all catalysts. From the result, we observed that the rate constant gradually increases from 0.01223 min^{-1} to 0.01856 min^{-1} when the doping of Cu^{+2} ions increasing from 0.5 % to 1 %, then decreasing and reached 0.00757 min^{-1} when the doping concentration reached 4 % Cu^{+2} ions. At all, the highest photocatalytic efficiency was observed for Cu doping ZnO compared to ZnO due to doping of Copper producing oxygen vacancy, decreasing size of the particle, decreasing the bandgap of the material which helps to extends the light absorption into visible light to harvest a large amount of solar light to generated numbers electron-holes pairs which attributed to degradation of organic dyes from the wastewater by forming reactive oxygen species such as superoxide radicals ($^oO^{-2}$), hydroxide radicals (^oOH), hydrogen peroxide

(H_2O_2).. In our result ,the reflectance of CZ-1 low in the visible light range which means a high visible absorbance than ZnO so, the photocatalytic activity of CZ-1 much better than ZnO. Therefore, the photocatalytic activity of pure ZnO was highly improved by doping Cu^{+2} ions. However, further increasing Cu doping reducing the photocatalytic activity due to producing secondary phase CuO in the small amount which was not contributing to enhancing photocatalytic activity, excess cu^{+2} ions acts the recombination of center for electrons -holes pairs(Kadam, Kim et al. 2017), which would suppress the photocatalytic activity of Cu doping ZnO at high concentration.

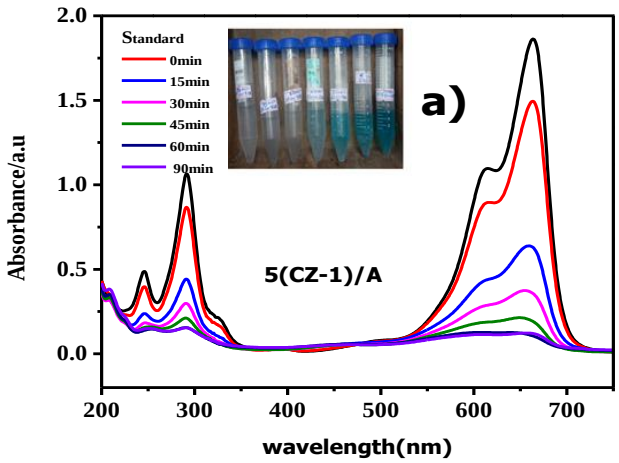

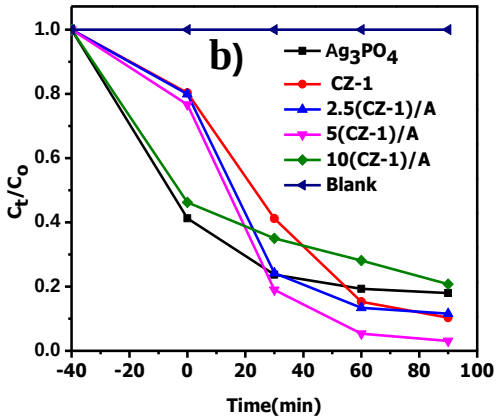

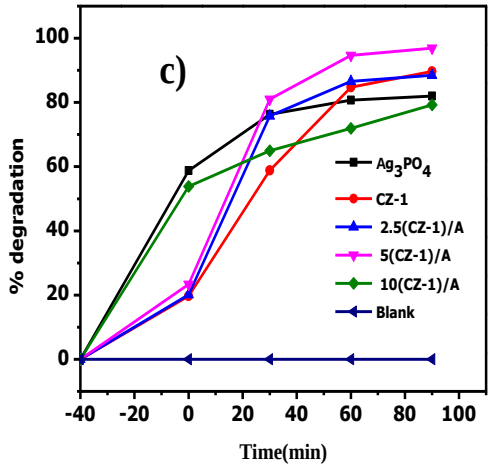

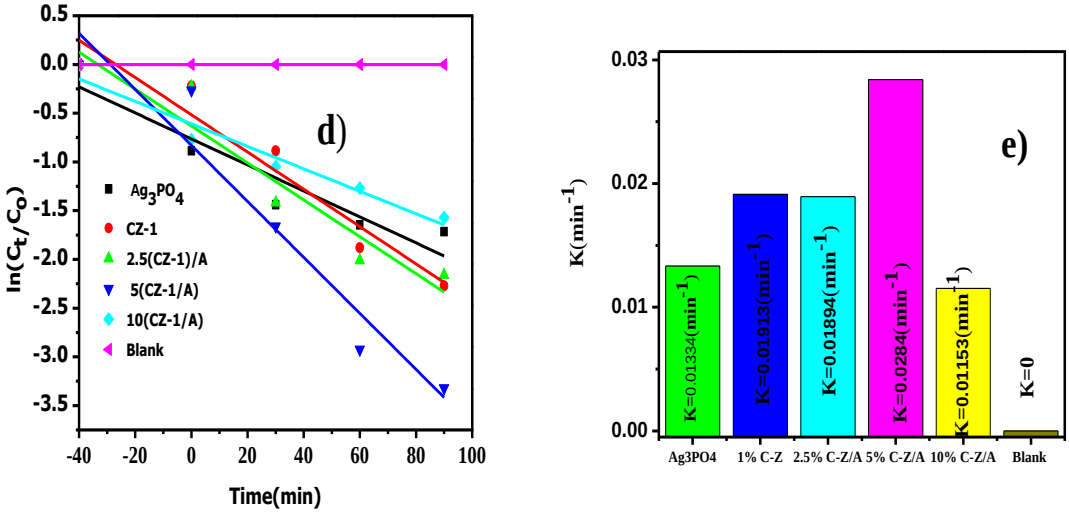

Figure:4.9 .The photo-degradation performance of MB for composite and single component .a) UV-Visible spectroscopy absorbance of MB for 5 (CZ-1)/A b) C_t/C_o vs time c) % degradation Vs time)d) Ln (Ct/Co) Vs time e) the rate constant for different catalyst.

In the above Fig 4.9, the photocatalytic activity of a single component and optimized composite were evaluated. As shown in Fig 4.9a,the absorption of a methylene blue inside the aqueous solution decreasing as the irradiation time of visible light increasing when 5(CZ-1)/A catalysts were added to the solution. Consequently, the color of the solution was gradually changed from blue to colorless pure water after 90 min. Fig 4.9b, and Fig 4.9c, indicated that the C_t/C_o versus irradiation time and degradation efficiency versus irradiation time for CZ-1, Ag_3PO_4, and for optimized y(CZ-1/A) (where y=2.5,5,10). C_t/C_o was decreasing when the time of irradiation was increasing, and also the efficiency of the degradation was increasing parallel. From the result, we investigated that the photocatalytic activity of 5(CZ-1)/A is higher than Ag_3PO_4, and CZ-1. Enticingly, degradation efficiency value for 5(CZ-1)/A), Ag_3PO_4, and CZ-1 was 95%, 82%, 88% respectively when irradiation time reached 90 min. In addition to this, the degradation efficiency of the composite increasing when the percentage of CZ-1 decorated on the Ag_3PO_4 were increasing from 2.5% to 5%. Nevertheless, the excess decoration of CZ-1 nanoparticles on the surface of Ag_3PO_4 was not further enhanced the photocatalytic activity of the composite due to shielding the absorption of the light by Ag_3PO_4 and hindering the dyes into active site materials(Chen, Dai et al. 2015). As a result, the degradation efficiency of 10(CZ-1)/A is lower than (CZ-1)/A.Fig4.9d,indicated that ln (C_t/C_o) versus irradiation time. ln (C_t/C_o)

decreasing linearly with irradiation time. From this, we clearly understand that degradation of methylene blue from aqueous solution could be fitted to pseudo-first-order kinetics.

The rate constant K (min^{-1}) of each component obtained was similar to the slope of the line corresponding catalyst. As listed in Fig 4.9e, the degradation rate was gradually increasing as the content of CZ-1 increased and reached the maximum value of 0.0284 min^{-1} at 5(CZ-1)/A composite and then diminishing to 0.01153 min^{-1} for 5(CZ-1)/A. So the 5(CZ-1)/A composite exhibits a higher photodegradation rate which was two times that of an original of Ag_3PO_4. The reason behind enhancing the photocatalytic activity of composite is decreasing of charge recombination of injected charge carriers between junction interface, due high absorption of light than single component by superposition of two materials , increasing of surface area when small size CZ-1 combined with large size of Ag_3PO_4 enhance degradation efficiency, and photo corrosion of the silver phosphate(Ag_3PO_4) suppressed by increasing the number of electrons transferring to the conduction band Ag_3PO_4 by facilitated multi-oxidation reaction and inhibit the formation large number of a black Ag^o nanoparticle which is causes for photocorrosion.. The same result was obtained by Ning et al which 5 %wt NiO/Ag_3PO_4 composite shows high photo removing for the methylene blue (MB) and RhB than a single component (Santos, Martins et al. 2020).

4.6.1. Effect of external factors

The plot C_t/C_o versus time in Fig 4.10a, shows the effect of catalyst dose on the removal efficiency of methylene blue inside an aqueous solution. From the result we investigated, increasing of catalyst amount from 0.222 g/L to 0.444 g/L were increasing the degradation efficiency of methylene blue from 94 % to 97 % due to increasing active site to harvest light by 5(CZ-1)/A, and generate many charge carriers which were attributed to the creation reactive oxygen species which was highly participating in a degradation activity. However, further increasing catalyst dose is decreasing the removal efficiency of dyes from aqueous solutions since the excess amount of catalyst inside the solution preventing or shielding the light to reach the active site to exciting electrons from the valance band to conduction due to turbidity of the solution and agglomeration the particle. Consequently, the removal efficiency of methylene blue (MB) decline for 0.666 g/L.The plot C_t/C_o in Fig 4.10b, reveals the effect of solution pH on photocatalytic activity. The degradation of methylene blue low at the acidic medium since the

composite surface charge is negative so that when it is imposed to acidic medium the surface was positively charged by protonated. As result, the degradation efficiency for cationic methylene blue was low owing to the electrostatic repulsion between surface positive charges and cationic dyes, and the surface becomes negative charge when 5(CZ-1)/A catalyst was imposed to basic medium. Therefore, the surface charge repels OH^- ions on the solution by electrostatic repulsion force, but the cationic methylene blue in the solution adsorbed to negatively charged surface by the phenomena of electrostatic attraction force. As a result, the removal efficiency of 5(CZ-1)/A for methylene blue high at pH=10 which was 95%, and low at pH=3 and pH=4 which is 54%, 80% respectively.

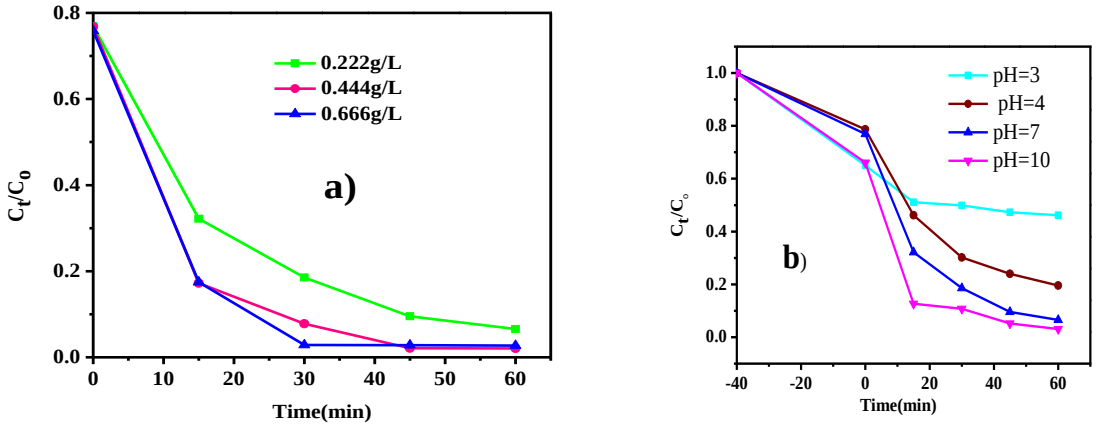

Figure:4.10. The effect of a) catalyst amount b) PH of the solution toward degradation of methylene blue from aqueous solution for 5(CZ-1)/A composite.

4.6.2. Recyclability and the possible Photocatalytic mechanism

Recyclability or reusability, stability issue of catalyst evaluated for three series by using 5(CZ-1)/A composite at 90 min.The experimental result indicated that in Fig 4.11a, the degradation efficiency of catalyst at first run, the second run, and the third run was 94.4%, 91.56%, 84.6%, respectively, but gradual decreasing of degradation efficiency may be due to the loss of catalyst during filtration, and also an agglomeration and sedimentation of the dyes after each run experiment around the active site of a catalyst were which the possible cause for decreasing degradation rate because at each run of photocatalysis needs a new surface catalyst for adsorption of dyes, so in this case, a new surface was unavailable for dye adsorption and

photon adsorption, resulted in decreasing of degradation efficiency catalyst(Taddesse, Alemu et al. 2020).

To study the possible mechanism of photocatalyst estimation of conduction band edge and valance band edge could be prominent, So the ECB and EVB edge was calculated by using Mulliken electronegativity formula as follows(Chen, Wang et al. 2013)

$$EVB = X - Eo + 0.5Eg \quad \text{.....4.7}$$

$$ECB = EVB - Eg \quad \text{..... 4.8}$$

Where as, X the absolute electronegativity of a given semiconductor, E_o is the energy of the free electron in the hydrogen scale (4.5 eV), and Eg the bandgap of the respective semiconductor. Electronegativity for Cu doped ZnO and Ag_3PO_4 could be 5.505(Bekkari, Laânab et al. 2020) and 5.965 (Taddesse, Alemu et al. 2020)respectively. So the calculated conduction band edge(ECB) and valance band edge (EVB) for Ag_3PO_4 and CZ-1 versus normal hydrogen electrode (NHE) could be 0.23 eV ,2.7 eV and -0.615 eV ,2.625 eV ,respectively. From the arrangement of band structure, we were understanding that the conduction band edge potential of Ag_3PO_4 much positive than the single-electron reduction process potential of (-0.046 eV), thus single-electron reduction for producing superoxide radicals ($^{\bullet}O_2^-$) did not take place on the conduction band of Ag_3PO_4. Based on the above value, a Z- scheme(type II) band structure arrangement was proposed to enhance the photocatalytic activity of the 5(CZ-1)/A composite which indicated in the following Fig 4.11b, Under visible light irradiation on the 5(CZ-1)/A composite the electron-hole pairs were generated in both single component of the composite, thereby the electron in the conduction band of CZ-1 plausible jumping to the conduction band of Ag_3PO_4 and reduced O_2 to superoxide radicals ($^{-o}O_2$) and degraded methylene blue (MB) to H_2O and CO_2 While the hole in the conduction band of Ag_3PO_4 transferring to the conduction band of CZ-1 so both phenomena attributed to suppressed the recombination of charge carriers. The excess electron on the conduction band of Ag_3PO_4 facilitated a multi oxidation reaction ($2e^- + O_2 + 2H^+ = H_2O_2$), and H_2O_2 further reacts with single electros ($H_2O_2 + e^- = {}^oOH$) form hydroxide radicals consequently, ^oOH radicals reacted with methylene blue and decomposed it into CO_2, H_2O, and non-toxic by-products. In this case photo corrosion of Ag_3PO_4 inhibited by the domination of the multi-oxidation process reaction than the combination Ag^+ ions with single electrons to form black Ag^o nanoparticle which the main

reason for an instability and photo corrosion of Ag_3PO_4.The holes in the valance band of Cu doped ZnO proceeded the two reactions to decompose of dye from an aqueous solution. The first reaction was h^+ directly reacted within organic dyes, and changed it in CO_2 and H_2O. In the second reaction, the hole reacted with H_2O and formed ^oOH radicals while it has been reacted with dyes, and decompose into carbon dioxide and water. Therefore, the overall mechanism in the 5(CZ-1)/A composite were improved the photocatalytic activity and instability of a single component. The detailed mechanism of the photocatalyst was illustrated in Fig 4.11b.

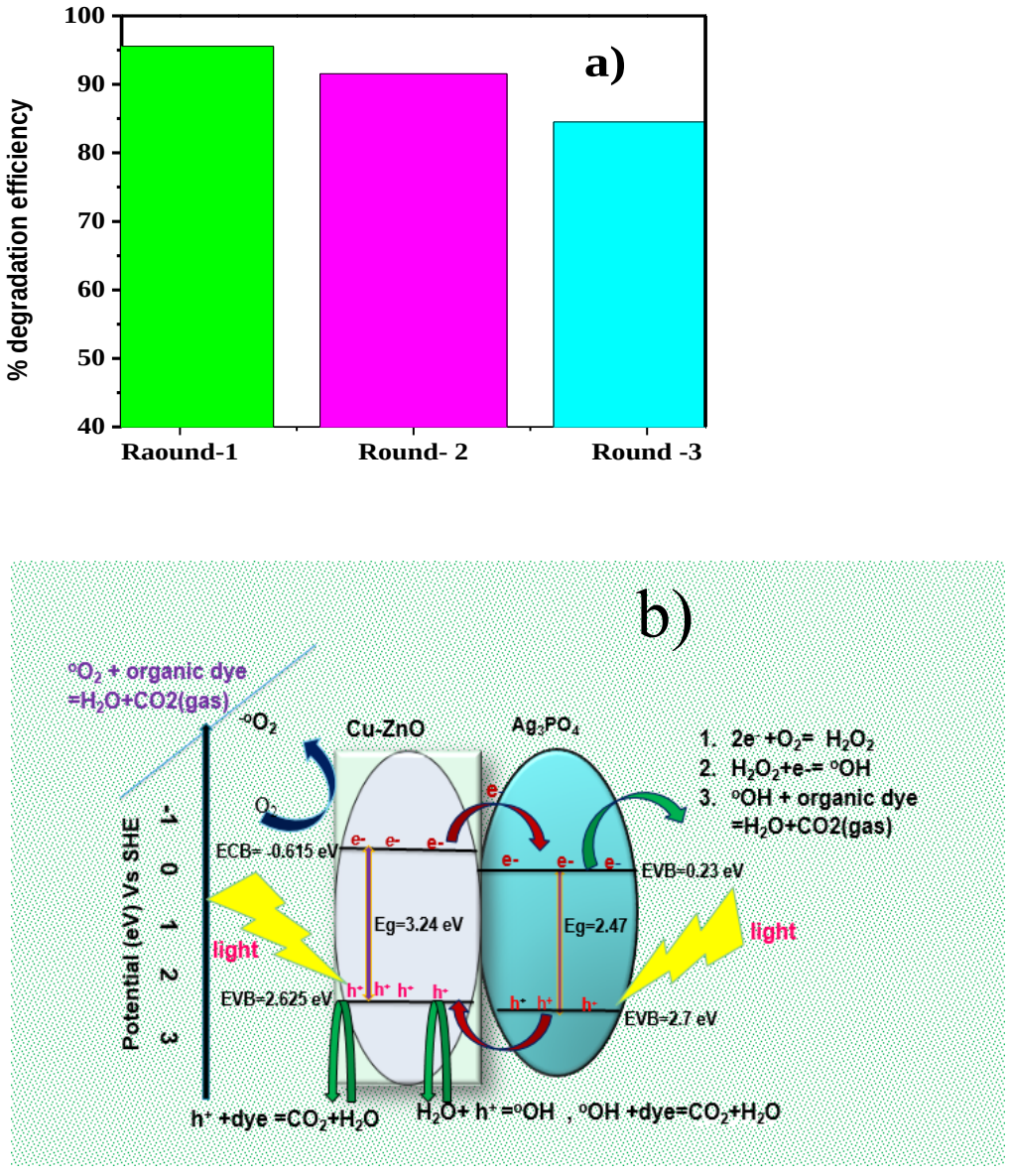

Figure: 4.11. (a)Reusability experiment (b)the photocatalytic mechanism of Cu-ZnO/Ag_3PO_4 composites systems

CONCLUSIONS AND RECOMMENDATIONS

Photocatalysis is a promising method to remove organic dyes from an aqueous solution Several semiconductor materials are used to degrade dyes among that Ag_3PO_4 best entrant photocatalyst to remove pollutants from wastewater ascribable to high absorption visible light (quantum efficiency up to 90%), but its acivity limited by photo corrosion, recombination of charge carriers. In this study, $Zn_{0.99}Cu_{0.01}O/Ag_3PO_4$ composite was synthesized by in situ precipitation methods. The light absorption of 5(CZ-1)/A composite high in the visible range than CZ-1 and Ag_3PO_4 while low recombination of charge carriers than single component because the absorption superposition of single component and charge transferring between the junction .As result , 5(CZ-1)/A showed good photocatalytic activity than other optimized composites such as 2.5(CZ-1)/A ,10(CZ-1/A) and single component .Where the degradation efficiency of 5(CZ-1)/A 94% . photo corrosion suppressed for Ag_3PO_4 by speed up multi-oxidation reaction at conduction bandgap of Ag_3PO_4. Results showed that the degradation efficiency of methylene blue(MB) achieved by 5(CZ-1)/A, Ag_3PO_4, and CZ-1 were 94%, 82%, 88% respectively. The pH value and catalyst dosage affect the removal efficiency of dyes. So 95% MB were removed at pH=10 owing to high adsorption of methylene blue (MB) to the negative surface of 5(CZ-1)/A catalyst as well as increasing of catalyst amount increased degradation activity due to many charge carriers were generated to produce reactive oxygen species to degrade dyes so, 97% methylene blue was removed at 0.0444g/L.Excess amount catalyst minimizing removal efficiency due to turbidity causes for light shielding. The Ag_3PO_4 calcined at 200 ^oC shows remarkable removal efficiency for methylene blue than pristine died at 100 ^oC and calcined at 300 ^oC,400 ^oC,500 ^oC,600 ^oC,600 ^oC owing to the low bandgap of Ag_3PO_4 and high absorption visible light and resulted in 98% methylene blue were degraded at 30min. Therefore, coupling of Cu doping ZnO with Ag_3PO_4 and calcined Ag_3PO_4 at 200 ^oC improved removing efficiency of methylene blue forAg_3PO_4.

Besides my work, I will recommend many works that lifted me to enhance the photocatalyst performance of Ag_3PO_4 in practical application.

1. The synthesizing parameters such as stirring time, synthesizing temperature, aging time, and different synthesizing methods did not discuss.

2. synthesizing of Ag_3PO_4 from waste by-products like Eggshell membrane(ESM) and bones which are the source of phosphate (PO^{4-})
3. The doping of large bandgap semiconductors (TiO_2 and ZnO) and coupling with Ag_3PO_4 did not study further.
4. Band modification of Ag_3PO_4 by doping has not been conducting, so it is one of the hot research areas in the future.
5. Decoration of various Noble metals and metal oxide semiconductors on different morphology Ag_3PO_4 is one of the insights in the future.
6. Coupling of Ag_3PO_4 with silicate-based material extracted from waste by-products of industry (e.g from .bagasse from sugar cane firm) and different silicate clay.
7. Synthesizing of ternary composite P-Co_3O_4/n-ZnO/Ag_3PO_4 did not conduct till now, this my future work if I get chance to conduct research.
8. Synthesizing of Ag_3PO_4 by using various natural extracted templates.

REFERENCE

Acharya, J., J. N. Sahu, B. K. Sahoo, C. R. Mohanty and B. C. Meikap (2009). "Removal of chromium(VI) from wastewater by activated carbon developed from Tamarind wood activated with zinc chloride." Chemical Engineering Journal **150**(1): 25-39.

Adam, R. E., G. Pozina, M. Willander and O. Nur (2018). "Synthesis of ZnO nanoparticles by co-precipitation method for solar driven photodegradation of Congo red dye at different pH." Photonics and Nanostructures - Fundamentals and Applications **32**: 11-18.

Akyol, A., H. C. Yatmaz and M. Bayramoglu (2004). "Photocatalytic decolorization of Remazol Red RR in aqueous ZnO suspensions." Applied Catalysis B: Environmental **54**(1): 19-24.

Al Kausor, M. and D. Chakrabortty (2020). "Facile fabrication of N-TiO_2/Ag_3PO_4@GO nanocomposite toward photodegradation of organic dye under visible light." Inorganic Chemistry Communications **116**: 107907.

Al Kausor, M., S. S. Gupta and D. Chakrabortty (2020). "Ag_3PO_4-based nanocomposites and their applications in photodegradation of toxic organic dye contaminated wastewater: Review on material design to performance enhancement." Journal of Saudi Chemical Society **24**(1): 20-41.

Alaria, J., P. Turek, M. Bernard, M. Bouloudenine, A. Berbadj, N. Brihi, G. Schmerber, S. Colis and A. Dinia (2005). "No ferromagnetism in Mn doped ZnO semiconductors." Chemical Physics Letters **415**(4): 337-341.

Allred, A. (1961). "Electronegativity values from thermochemical data." Journal of inorganic and nuclear chemistry **17**(3-4): 215-221.

Amornpitoksuk, P. and S. Suwanboon (2014). "Photocatalytic decolorization of methylene blue dye by Ag_3PO_4–AgX (X=Cl−, Br− and I−) under visible light." Advanced Powder Technology **25**(3): 1026-1030.

Asahi, R., T. Morikawa, T. Ohwaki, K. Aoki and Y. Taga (2001). "Visible-light photocatalysis in nitrogen-doped titanium oxides." Science **293**(5528): 269-271.

Ashokkumar, M. and S. Muthukumaran (2015). "Electrical, dielectric, photoluminescence and magnetic properties of ZnO nanoparticles co-doped with Co and Cu." Journal of Magnetism and Magnetic Materials **374**: 61-66.

Asrofi, M., H. Abral, A. Kasim and A. Pratoto (2017). "XRD and FTIR Studies of Nanocrystalline Cellulose from Water Hyacinth (Eichornia crassipes) Fiber." Journal of Metastable and Nanocrystalline Materials **29**: 9-16.

Aziz, H. A., S. Alias, M. N. Adlan, Faridah, A. H. Asaari and M. S. Zahari (2007). "Colour removal from landfill leachate by coagulation and flocculation processes." Bioresour Technol **98**(1): 218-220.

Banu Bahşi, Z. and A. Y. Oral (2007). "Effects of Mn and Cu doping on the microstructures and optical properties of sol–gel derived ZnO thin films." Optical Materials **29**(6): 672-678.

Barakat, M. A. (2011). "New trends in removing heavy metals from industrial wastewater." Arabian Journal of Chemistry **4**(4): 361-377.

Behjati, S., S. Sheibani, J. Herritsch and J. M. Gottfried (2020). "Photodegradation of dyes in batch and continuous reactors by Cu_2O-CuO nano-photocatalyst on Cu foils prepared by chemical-thermal oxidation." Materials Research Bulletin **130**: 110920.

Bekkari, R., L. Laânab and B. Jaber (2020). "Effect of the bivalent dopant ionic radius, electronegativity and concentration on the physical properties of the sol–gel-derived ZnO thin films." Journal of Materials Science: Materials in Electronics **31**(18): 15129-15139.

Beltrán, J. J., C. A. Barrero and A. Punnoose (2016). "Combination of Defects Plus Mixed Valence of Transition Metals: A Strong Strategy For Ferromagnetic Enhancement in ZnO Nanoparticles." The Journal of Physical Chemistry C **120**(16): 8969-8978.
Bi, Y., H. Hu, S. Ouyang, Z. Jiao, G. Lu and J. Ye (2012). "Selective growth of Ag_3PO_4 submicro-cubes on Ag nanowires to fabricate necklace-like heterostructures for photocatalytic applications." Journal of Materials Chemistry **22**(30): 14847.
Bouras, D., A. Mecif, R. Barillé, A. Harabi, M. Rasheed, A. Mahdjoub and M. Zaabat (2018). "Cu:ZnO deposited on porous ceramic substrates by a simple thermal method for photocatalytic application." Ceramics International **44**(17): 21546-21555.
Chandekar, K. V., M. Shkir, B. M. Al-Shehri, S. AlFaify, R. G. Halor, A. Khan, K. S. Al-Namshah and M. S. Hamdy (2020). "Visible light sensitive Cu doped ZnO: Facile synthesis, characterization and high photocatalytic response." Materials Characterization **165**: 110387.
Chen, H. and K. C. Carroll (2016). "Metal-free catalysis of persulfate activation and organic-pollutant degradation by nitrogen-doped graphene and aminated graphene." Environmental Pollution **215**: 96-102.
Chen, H., Z. Zhao, Z. Chen, J. Yi, K. Xia, H. Xu, M. Chen and H. Li (2018). "Co_3O_4 nanoparticles decorated Ag3PO4 as heterostructure for improving solar-light-driven photocatalysis." IOP Conference Series: Earth and Environmental Science **199**: 032087.
Chen, J., X.-P. Liu, X.-D. Yang, L.-L. Jiang, C.-J. Mao, H. Niu, B.-K. Jin and S. Zhang (2017). "A novel Ag_3PO_4/CuO nanocomposite with enhanced photocatalytic performance." Materials Letters **188**: 300-303.
Chen, J., X.-P. Liu, X.-D. Yang, L.-L. Jiang, C.-J. Mao, H. Niu, B.-K. Jin and S. Zhang (2017). "A novel Ag 3 PO 4 /CuO nanocomposite with enhanced photocatalytic performance." Materials Letters **188**: 300-303.
Chen, X., Y. Dai, T. Liu, J. Guo, X. Wang and F. Li (2015). "Magnetic core–shell carbon microspheres (CMSs)@$ZnFe_2O_4$/Ag_3PO_4 composite with enhanced photocatalytic activity and stability under visible light irradiation." Journal of Molecular Catalysis A: Chemical **409**: 198-206.
Chen, Z., W. Wang, Z. Zhang and X. Fang (2013). "High-Efficiency Visible-Light-Driven Ag_3PO_4/AgI Photocatalysts: Z-Scheme Photocatalytic Mechanism for Their Enhanced Photocatalytic Activity." The Journal of Physical Chemistry C **117**(38): 19346-19352.
Chong, R., X. Cheng, B. Wang, D. Li, Z. Chang and L. Zhang (2016). "Enhanced photocatalytic activity of Ag $_3$ PO $_4$ for oxygen evolution and Methylene blue degeneration: Effect of calcination temperature." International Journal of Hydrogen Energy **41**(4): 2575-2582.
Coleman, H. M., V. Vimonses, G. Leslie and R. Amal (2007). "Degradation of 1,4-dioxane in water using TiO_2 based photocatalytic and H_2O_2/UV processes." J Hazard Mater **146**(3): 496-501.
Deng, Y. and R. Zhao (2015). "Advanced Oxidation Processes (AOPs) in Wastewater Treatment." Current Pollution Reports **1**(3): 167-176.
Dhanabal, R., A. Chithambararaj, S. Velmathi and A. C. Bose (2015). "Visible light driven degradation of methylene blue dye using Ag_3PO_4." Journal of Environmental Chemical Engineering **3**(3): 1872-1881.
Diouri, J., J. P. Lascaray and M. E. Amrani (1985). "Effect of the magnetic order on the optical-absorption edge in Cd1-xMnxTe." Phys Rev B Condens Matter **31**(12): 7995-7999.
Dodoo-Arhin, D., F. P. Buabeng, J. M. Mwabora, P. N. Amaniampong, H. Agbe, E. Nyankson, D. O. Obada and N. Y. Asiedu (2018). "The effect of titanium dioxide synthesis technique and its photocatalytic degradation of organic dye pollutants." Heliyon **4**(7): e00681.

Dong, P., G. Hou, C. Liu, X. Zhang, H. Tian, F. Xu, X. Xi and R. Shao (2016). "Origin of Activity and Stability Enhancement for $Ag_{(3)}PO_{(4)}$ Photocatalyst after Calcination." Materials (Basel) **9**(12).
Du, C., J. Song, S. Tan, L. Yang, G. Yu, H. Chen, L. Zhou, Z. Zhang, Y. Zhang, Y. Su, X. Wen and S. Wang (2021). "Facile synthesis of Z-scheme ZnO/Ag/Ag_3PO_4 composite photocatalysts with enhanced performance for the degradation of ciprofloxacin." Materials Chemistry and Physics **260**: 124136.
Dwivedi, S., S. Mishra and R. D. Tripathi (2018). "Ganga water pollution: A potential health threat to inhabitants of Ganga basin." Environ Int **117**: 327-338.
Egbueri, J. C. (2020). "Heavy Metals Pollution Source Identification and Probabilistic Health Risk Assessment of Shallow Groundwater in Onitsha, Nigeria." Analytical Letters **53**(10): 1620-1638.
Elhalil, A., R. Elmoubarki, M. Farnane, A. Machrouhi, M. Sadiq, F. Z. Mahjoubi, S. Qourzal and N. Barka (2018). "Photocatalytic degradation of caffeine as a model pharmaceutical pollutant on Mg doped ZnO-Al2O3 heterostructure." Environmental Nanotechnology, Monitoring & Management **10**: 63-72.
Evans, A. E. V., J. Mateo-Sagasta, M. Qadir, E. Boelee and A. Ippolito (2019). "Agricultural water pollution: key knowledge gaps and research needs." Current Opinion in Environmental Sustainability **36**: 20-27.
Fujishima, A. and K. Honda (1972). "Electrochemical Photolysis of Water at a Semiconductor Electrode." Nature **238**(5358): 37-38.
Gaya, U. I. and A. H. Abdullah (2008). "Heterogeneous photocatalytic degradation of organic contaminants over titanium dioxide: A review of fundamentals, progress and problems." Journal of Photochemistry and Photobiology C: Photochemistry Reviews **9**(1): 1-12.
Ge, M., N. Zhu, Y. Zhao, J. Li and L. Liu (2012). "Sunlight-Assisted Degradation of Dye Pollutants in Ag_3PO_4 Suspension." Industrial & Engineering Chemistry Research **51**(14): 5167-5173.
Giovannetti, R., E. Rommozzi, C. D'Amato and M. Zannotti (2016). "Kinetic Model for Simultaneous Adsorption/Photodegradation Process of Alizarin Red S in Water Solution by Nano-TiO_2 under Visible Light." Catalysts **6**(6): 84.
Guivarch, E., S. Trevin, C. Lahitte and M. A. Oturan (2003). "Degradation of azo dyes in water by Electro-Fenton process." Environmental Chemistry Letters **1**(1): 38-44.
Gunkel, G., J. Kosmol, M. Sobral, H. Rohn, S. Montenegro and J. Aureliano (2006). "Sugar Cane Industry as a Source of Water Pollution – Case Study on the Situation in Ipojuca River, Pernambuco, Brazil." Water, Air, and Soil Pollution **180**(1-4): 261-269.
Guo, J., H. Shi, X. Huang, H. Shi and Z. An (2018). "AgCl/Ag_3PO_4: A stable Ag-Based nanocomposite photocatalyst with enhanced photocatalytic activity for the degradation of parabens." J Colloid Interface Sci **515**: 10-17.
Hepel, M. and S. Hazelton (2005). "Photoelectrocatalytic degradation of diazo dyes on nanostructured WO_3 electrodes." Electrochimica Acta **50**(25): 5278-5291.
Hollender, J., S. G. Zimmermann, S. Koepke, M. Krauss, C. S. McArdell, C. Ort, H. Singer, U. von Gunten and H. Siegrist (2009). "Elimination of Organic Micropollutants in a Municipal Wastewater Treatment Plant Upgraded with a Full-Scale Post-Ozonation Followed by Sand Filtration." Environmental Science & Technology **43**(20): 7862-7869.
Homlok, R., G. Kiskó, A. Kovács, T. Tóth, E. Takács, C. Mohácsi-Farkas, L. Wojnárovits and L. Szabó (2021). "Antibiotics in a wastewater matrix at environmentally relevant concentrations

affect coexisting resistant/sensitive bacterial cultures with profound impact on advanced oxidation treatment." Science of The Total Environment **754**: 142181.
Hu, H., M. Yang and J. Dang (2005). "Treatment of strong acid dye wastewater by solvent extraction." Separation and Purification Technology **42**(2): 129-136.
Iribarren, A., E. Hernández-Rodríguez and L. Maqueira (2014). "Structural, chemical and optical evaluation of Cu-doped ZnO nanoparticles synthesized by an aqueous solution method." Materials Research Bulletin **60**: 376-381.
Jeyachitra, R., V. Senthilnathan and T. S. Senthil (2017). "Studies on electrical behavior of Fe doped ZnO nanoparticles prepared via co-precipitation approach for photo-catalytic application." Journal of Materials Science: Materials in Electronics **29**(2): 1189-1197.
Jin, Z., T. Fukumura, M. Kawasaki, K. Ando, H. Saito, T. Sekiguchi, Y. Z. Yoo, M. Murakami, Y. Matsumoto, T. Hasegawa and H. Koinuma (2001). "High throughput fabrication of transition-metal-doped epitaxial ZnO thin films: A series of oxide-diluted magnetic semiconductors and their properties." Applied Physics Letters **78**(24): 3824-3826.
Jun, B.-M., Y. Kim, Y. Yoon, Y. Yea and C. M. Park (2020). "Enhanced sonocatalytic degradation of recalcitrant organic contaminants using a magnetically recoverable Ag/Fe-loaded activated biochar composite." Ceramics International **46**(14): 22521-22531.
Kadam, A. N., T. G. Kim, D. S. Shin, K. M. Garadkar and J. Park (2017). "Morphological evolution of Cu doped ZnO for enhancement of photocatalytic activity." Journal of Alloys and Compounds **710**: 102-113.
Karimi, L., S. Zohoori and M. E. Yazdanshenas (2014). "Photocatalytic degradation of azo dyes in aqueous solutions under UV irradiation using nano-strontium titanate as the nanophotocatalyst." Journal of Saudi Chemical Society **18**(5): 581-588.
Katsumata, H., Y. Oda, S. Kaneco and T. Suzuki (2013). "Photocatalytic activity of Ag/CuO/WO_3 under visible-light irradiation." RSC Advances **3**(15): 5028.
Khomenko, S., M. Cirach, E. Pereira-Barboza, N. Mueller, J. Barrera-Gómez, D. Rojas-Rueda, K. de Hoogh, G. Hoek and M. Nieuwenhuijsen (2021). "Premature mortality due to air pollution in European cities: a health impact assessment." The Lancet Planetary Health **5**(3): e121-e134.
Kim, D. Y., S.-O. Kim, M. S. Kim, K. G. Yim, J.-Y. Leem, S. Kim, G. Nam and D.-Y. Lee (2012). "Hydrothermal growth and properties of rod-like ZnO submicron crystals on Al-doped ZnO seed layers with different Al concentrations." Journal of the Korean Physical Society **60**(1): 94-98.
Kim, K. J. and Y. R. Park (2002). "Spectroscopic ellipsometry study of optical transitions in Zn1−xCoxO alloys." Applied Physics Letters **81**(8): 1420-1422.
Konstantinou, I. K. and T. A. Albanis (2004). "TiO2-assisted photocatalytic degradation of azo dyes in aqueous solution: kinetic and mechanistic investigations." Applied Catalysis B: Environmental **49**(1): 1-14.
Kulyk, B., B. Sahraoui, V. Figà, B. Turko, V. Rudyk and V. Kapustianyk (2009). "Influence of Ag, Cu dopants on the second and third harmonic response of ZnO films." Journal of Alloys and Compounds **481**(1): 819-825.
Kumar, A. and G. Pandey (2017). "Photocatalytic degradation of Eriochrome Black-T by the Ni:TiO_2 nanocomposites." Desalination and Water Treatment **71**: 406-419.
Kundu, S., A. Pal and A. K. Dikshit (2005). "UV induced degradation of herbicide 2,4-D: kinetics, mechanism and effect of various conditions on the degradation." Separation and Purification Technology **44**(2): 121-129.

Lebogang, L., R. Bosigo, K. Lefatshe and C. Muiva (2019). "Ag_3PO_4/nanocellulose composite for effective sunlight driven photodegradation of organic dyes in wastewater." Materials Chemistry and Physics **236**: 121756.
Lee, S.-Y. and S.-J. Park (2013). "TiO2 photocatalyst for water treatment applications." Journal of Industrial and Engineering Chemistry **19**(6): 1761-1769.
Li, J., W. Fang, C. Yu, W. Zhou, L. zhu and Y. Xie (2015). "Ag-based semiconductor photocatalysts in environmental purification." Applied Surface Science **358**: 46-56.
Li, P., J. Jing, W. Guo, X. Guo, W. Hu, X. Qi, W.-Q. Wei and G. Zhuang (2021). "The associations of air pollution and socioeconomic factors with esophageal cancer in China based on a spatiotemporal analysis." Environmental Research **196**: 110415.
Li, X.-Y., H.-J. Li, M. Yuan, Z.-J. Wang, Z.-Y. Zhou and R.-B. Xu (2011). "Influence of oxygen partial pressure on electrical and optical properties of Zn0.93Mn0.07O thin films." Journal of Alloys and Compounds **509**(6): 3025-3031.
Lin, J., M. Guo, C. T. Yip, W. Lu, G. Zhang, X. Liu, L. Zhou, X. Chen and H. Huang (2013). "High Temperature Crystallization of Free-Standing Anatase TiO_2Nanotube Membranes for High Efficiency Dye-Sensitized Solar Cells." Advanced Functional Materials **23**(47): 5952-5960.
Liu, J. J., X. L. Fu, S. F. Chen and Y. F. Zhu (2011). "Electronic structure and optical properties of Ag_3PO_4 photocatalyst calculated by hybrid density functional method." Applied Physics Letters **99**(19): 191903.
Liu, Y., J. Yang, Q. Guan, L. Yang, Y. Zhang, Y. Wang, B. Feng, J. Cao, X. Liu, Y. Yang and M. Wei (2009). "Effects of Cr-doping on the optical and magnetic properties in ZnO nanoparticles prepared by sol–gel method." Journal of Alloys and Compounds **486**(1): 835-838.
Liu, Z.-L., J.-C. Deng, J.-J. Deng and F.-F. Li (2008). "Fabrication and photocatalysis of CuO/ZnO nano-composites via a new method." Materials Science and Engineering: B **150**(2): 99-104.
Luis Sánchez-Salas, J., A. Aguilar Ubeda, B. Flores Gómez, O. Daniel Máynez Navarro, M. Ángel Méndez Rojas, S. Reyna Tellez and E. R. Bandala (2017). "Inactivation of Bacterial Spores and Vegetative Bacterial Cells by Interaction with ZnO-Fe₂O₃ Nanoparticles and UV Radiation." AIMS Geosciences **3**(4): 498-513.
Luo, J., G. Duan, W. Wang, Y. Luo and X. Liu (2017). "Size-controlled synthesis of palygorskite/Ag $_3$ PO $_4$ nanocomposites with enhanced visible-light photocatalytic performance." Applied Clay Science **143**: 273-278.
Luo, L., Y. Li, J. Hou and Y. Yang (2014). "Visible photocatalysis and photostability of Ag_3PO_4 photocatalyst." Applied Surface Science **319**: 332-338.
Luo, Y., N. Xu, X. Liu, L. Yang, H. Wu and Y. Qin (2015). "Photoactivity Enhanced and Photo-Corrosion Inhibited Ag_3PO_4/ZnO Visible Light Photocatalyst for the Degradation of Rhodamine B." Energy and Environment Focus **4**(2): 121-127.
Ma, D., H. Yi, C. Lai, X. Liu, X. Huo, Z. An, L. Li, Y. Fu, B. Li, M. Zhang, L. Qin, S. Liu and L. Yang (2021). "Critical review of advanced oxidation processes in organic wastewater treatment." Chemosphere **275**: 130104.
Ma, Z., F. Ren, X. Ming, Y. Long and A. A. Volinsky (2019). "Cu-Doped ZnO Electronic Structure and Optical Properties Studied by First-Principles Calculations and Experiments." Materials (Basel) **12**(1).
Maione, M., E. Mocca, K. Eisfeld, Y. Kazepov and S. Fuzzi (2021). "Public perception of air pollution sources across Europe." Ambio **50**(6): 1150-1158.

Mamba, G., M. A. Mamo, X. Y. Mbianda and A. K. Mishra (2014). "Nd,N,S-TiO_2 Decorated on Reduced Graphene Oxide for a Visible Light Active Photocatalyst for Dye Degradation: Comparison to Its MWCNT/Nd,N,S-TiO_2 Analogue." Industrial & Engineering Chemistry Research **53**(37): 14329-14338.
Martín-Gómez, A. N., J. A. Navío, C. Jaramillo-Páez, P. Sánchez-Cid and M. C. Hidalgo (2020). "Hybrid ZnO/Ag_3PO_4 photocatalysts, with low and high phosphate molar percentages." Journal of Photochemistry and Photobiology A: Chemistry **388**: 112196.
Martínez-Costa, J. I., J. Rivera-Utrilla, R. Leyva-Ramos, M. Sánchez-Polo, I. Velo-Gala and A. J. Mota (2018). "Individual and simultaneous degradation of the antibiotics sulfamethoxazole and trimethoprim in aqueous solutions by Fenton, Fenton-like and photo-Fenton processes using solar and UV radiations." Journal of Photochemistry and Photobiology A: Chemistry **360**: 95-108.
Martinez-Huitle, C. A. and E. Brillas (2009). "Decontamination of Wastewaters Containing Synthetic Organic Dyes by Electrochemical Methods: A General Review." Applied Catalysis B-environmental - APPL CATAL B-ENVIRON **87**: 105-145.
Mathew, M., S. C. Rosary, M. Sebastian and S. M. Cherian (2016). "Effectiveness of Vetiver System for the Treatment of Wastewater from an Institutional Kitchen." Procedia Technology **24**: 203-209.
Meng, Z. and Z. Juan (2008). "Wastewater treatment by photocatalytic oxidation of Nano-ZnO."
Miklos, D. B., C. Remy, M. Jekel, K. G. Linden, J. E. Drewes and U. Hübner (2018). "Evaluation of advanced oxidation processes for water and wastewater treatment – A critical review." Water Research **139**: 118-131.
Miyauchi, M., A. Nakajima, T. Watanabe and K. Hashimoto (2002). "Photocatalysis and Photoinduced Hydrophilicity of Various Metal Oxide Thin Films." Chemistry of Materials **14**(6): 2812-2816.
Muthukumaran, S. and R. Gopalakrishnan (2012). "Structural, FTIR and photoluminescence studies of Cu doped ZnO nanopowders by co-precipitation method." Optical Materials **34**(11): 1946-1953.
Noda, Y., B. Lee, K. Domen and J. N. Kondo (2008). "Synthesis of Crystallized Mesoporous Tantalum Oxide and Its Photocatalytic Activity for Overall Water Splitting under Ultraviolet Light Irradiation." Chemistry of Materials **20**(16): 5361-5367.
Nyankson, E. and R. V. Kumar (2019). "Removal of water-soluble dyes and pharmaceutical wastes by combining the photocatalytic properties of Ag_3PO_4 with the adsorption properties of halloysite nanotubes." Materials Today Advances **4**: 100025.
Parvulescu, V. I. and P. Granger (2013). Chapter 17 - Current Heterogeneous Catalytic Processes for Environmental Remediation of Air, Water, and Soil. New and Future Developments in Catalysis. S. L. Suib. Amsterdam, Elsevier**:** 487-534.
Pirhashemi, M. and A. Habibi-Yangjeh (2014). "Preparation of AgCl–ZnO nanocomposites as highly efficient visible-light photocatalysts in water by one-pot refluxing method." Journal of Alloys and Compounds **601**: 1-8.
Rajeshwar, K., M. E. Osugi, W. Chanmanee, C. R. Chenthamarakshan, M. V. B. Zanoni, P. Kajitvichyanukul and R. Krishnan-Ayer (2008). "Heterogeneous photocatalytic treatment of organic dyes in air and aqueous media." Journal of Photochemistry and Photobiology C: Photochemistry Reviews **9**(4): 171-192.
Rehman, S., R. Ullah, A. M. Butt and N. D. Gohar (2009). "Strategies of making TiO2 and ZnO visible light active." J Hazard Mater **170**(2-3): 560-569.

Reza, K. M., A. S. W. Kurny and F. Gulshan (2015). "Parameters affecting the photocatalytic degradation of dyes using TiO_2: a review." Applied Water Science **7**(4): 1569-1578.
Rout, P. R., T. C. Zhang, P. Bhunia and R. Y. Surampalli (2021). "Treatment technologies for emerging contaminants in wastewater treatment plants: A review." Science of The Total Environment **753**: 141990.
Ruzmanova, Y., M. Stoller and A. Chianese (2013). "Photocatalytic Treatment of Olive Mill Wastewater by Magnetic Core Titanium Dioxide Nanoparticles." Chemical Engineering Transactions **32**: 2269-2274.
Samsudin, E. M., N. G. Sze, Y. W. Ta, T. L. Tan, S. B. Abd. Hamid and C. J. Joon (2015). "Evaluation on the Photocatalytic Degradation Activity of Reactive Blue 4 using Pure Anatase Nano-TiO_2." Sains Malaysiana **44**(7): 1011-1019.
Santos, R. K., T. A. Martins, G. N. Silva, M. V. S. Conceicao, I. C. Nogueira, E. Longo and G. Botelho (2020). "Ag_3PO_4/NiO Composites with Enhanced Photocatalytic Activity under Visible Light." ACS Omega **5**(34): 21651-21661.
Saravanan, R., F. Gracia and A. Stephen (2017). "Basic Principles, Mechanism, and Challenges of Photocatalysis." 19-40.
Serrà, A., E. Gómez, J. Michler and L. Philippe (2020). "Facile cost-effective fabrication of Cu@Cu_2O@CuO–microalgae photocatalyst with enhanced visible light degradation of tetracycline." Chemical Engineering Journal: 127477.
Shan, A. Y., T. I. M. Ghazi and S. A. Rashid (2010). "Immobilisation of titanium dioxide onto supporting materials in heterogeneous photocatalysis: A review." Applied Catalysis A: General **389**(1): 1-8.
Simimol, A., A. A. Anappara and H. C. Barshilia (2017). "Influence of defects on electrical properties of electrodeposited co-doped ZnO nanocoatings." Materials Research Express **4**(1): 015001.
Sluiter, M. H., Y. Kawazoe, P. Sharma, A. Inoue, A. R. Raju, C. Rout and U. V. Waghmare (2005). "First principles based design and experimental evidence for a ZnO-based ferromagnet at room temperature." Phys Rev Lett **94**(18): 187204.
Song, X. C., Y. L. Qi, Y. F. Zheng, J. N. Liu and H. Y. Yin (2017). "Construction of Magnetic $Fe_{(3)}O_{(4)}$@C@$Ag_{(3)}PO_{(4)}$ Nanocomposites with Excellent Visible Photocatalytic Performance." J Nanosci Nanotechnol **17**(2): 1407-1412.
Sörme, L. and R. Lagerkvist (2002). "Sources of Heavy Metals in Urban Wastewater in Stockholm." The Science of the total environment **298**: 131-145.
Su, X., W. Chen, Y. Han, D. Wang and J. Yao (2021). "In-situ synthesis of Cu_2O on cotton fibers with antibacterial properties and reusable photocatalytic degradation of dyes." Applied Surface Science **536**: 147945.
Sun, J., L. Pan, D. C. W. Tsang, Y. Zhan, W. Liu, X. Wang, L. Zhu and X. Li (2016). "Polychlorinated biphenyls in agricultural soils from the Yangtze River Delta of China: Regional contamination characteristics, combined ecological effects and human health risks." Chemosphere **163**: 422-428.
Sun, T.-W., Y.-J. Zhu, C. Qi, G.-J. Ding, F. Chen and J. Wu (2016). "α-Fe_2O_3 nanosheet-assembled hierarchical hollow mesoporous microspheres: Microwave-assisted solvothermal synthesis and application in photocatalysis." Journal of Colloid and Interface Science **463**: 107-117.
Taddesse, A. M., M. Alemu and T. Kebede (2020). "Enhanced photocatalytic activity of p-n-n heterojunctions ternary composite Cu_2O/ZnO/Ag_3PO_4 under visible light irradiation." Journal of Environmental Chemical Engineering **8**(5): 104356.

Tang, C., E. Liu, J. Wan, X. Hu and J. Fan (2016). "Co_3O_4 nanoparticles decorated Ag_3PO_4 tetrapods as an efficient visible-light-driven heterojunction photocatalyst." Applied Catalysis B: Environmental **181**: 707-715.
Tao, Y. M., S. Y. Ma, H. X. Chen, J. X. Meng, L. L. Hou, Y. F. Jia and X. R. Shang (2011). "Effect of the oxygen partial pressure on the microstructure and optical properties of ZnO:Cu films." Vacuum **85**(7): 744-748.
Teng, W., X. Li, Q. Zhao, J. Zhao and D. Zhang (2012). "In situ capture of active species and oxidation mechanism of RhB and MB dyes over sunlight-driven Ag/Ag_3PO_4 plasmonic nanocatalyst." Applied Catalysis B: Environmental **125**: 538-545.
Umezawa, N., O. Shuxin and J. Ye (2011). "Theoretical study of high photocatalytic performance of Ag_3PO_4." Physical Review B **83**(3).
Vijayaprasath, G., R. Murugan, T. Mahalingam and G. Ravi (2015). "Comparative study of structural and magnetic properties of transition metal (Co, Ni) doped ZnO nanoparticles." Journal of Materials Science: Materials in Electronics **26**(9): 7205-7213.
Wang, H., Y. Bai, J. Yang, X. Lang, J. Li and L. Guo (2012). "A facile way to rejuvenate Ag_3PO_4 as a recyclable highly efficient photocatalyst." Chemistry **18**(18): 5524-5529.
Wang, P., Y. Li, Z. Liu, J. Chen, Y. Wu, M. Guo and P. Na (2017). "In-situ deposition of Ag_3PO_4 on TiO_2 nanosheets dominated by (001) facets for enhanced photocatalytic activities and recyclability." Ceramics International **43**(15): 11588-11595.
Wang, Q. and Z. Yang (2016). "Industrial water pollution, water environment treatment, and health risks in China." Environ Pollut **218**: 358-365.
Wei, Z., Q. Van Le, W. Peng, Y. Yang, H. Yang, H. Gu, S. S. Lam and C. Sonne (2021). "A review on phytoremediation of contaminants in air, water and soil." Journal of Hazardous Materials **403**: 123658.
Wu, S., H. Cao, S. Yin, X. Liu and X. Zhang (2009). "Amino Acid-Assisted Hydrothermal Synthesis and Photocatalysis of SnO_2 Nanocrystals." The Journal of Physical Chemistry C **113**(41): 17893-17898.
Xiang, Q., D. Lang, T. Shen and F. Liu (2015). "Graphene-modified nanosized Ag_3PO_4 photocatalysts for enhanced visible-light photocatalytic activity and stability." Applied Catalysis B: Environmental **162**: 196-203.
Yan, T., H. Zhang, Y. Liu, W. Guan, J. Long, W. Li and J. You (2014). "Fabrication of robust M/Ag_3PO_4(M = Pt, Pd, Au) Schottky-type heterostructures for improved visible-light photocatalysis." RSC Advances **4**(70): 37220.
Yang, J., M. Wang, S. Zhao, Y. Liu, W. Zhang, B. Wu and Q. Liu (2019). "Petal-biotemplated synthesis of two-dimensional Co_3O_4 nanosheets as photocatalyst with enhanced photocatalytic activity." International Journal of Hydrogen Energy **44**(2): 870-879.
Yassıtepe, E., H. C. Yatmaz, C. Öztürk, K. Öztürk and C. Duran (2008). "Photocatalytic efficiency of ZnO plates in degradation of azo dye solutions." Journal of Photochemistry and Photobiology A: Chemistry **198**(1): 1-6.
Yi, Z., J. Ye, N. Kikugawa, T. Kako, S. Ouyang, H. Stuart-Williams, H. Yang, J. Cao, W. Luo, Z. Li, Y. Liu and R. L. Withers (2010). "An orthophosphate semiconductor with photooxidation properties under visible-light irradiation." Nat Mater **9**(7): 559-564.
Yi, Z., J. Ye, N. Kikugawa, T. Kako, S. Ouyang, H. Stuart-Williams, H. Yang, J. Cao, W. Luo, Z. Li, Y. Liu and R. L. Withers (2010). "An orthophosphate semiconductor with photooxidation properties under visible-light irradiation." Nature Materials **9**(7): 559-564.
Yu, J.-G., H.-G. Yu, B. Cheng, X.-J. Zhao, J. C. Yu and W.-K. Ho (2003). "The Effect of Calcination Temperature on the Surface Microstructure and Photocatalytic Activity of TiO_2

Thin Films Prepared by Liquid Phase Deposition." The Journal of Physical Chemistry B **107**(50): 13871-13879.
Yu, Y., B. Yao, Y. He, B. Cao, Y. Ren and Q. Sun (2020). "Piezo-enhanced photodegradation of organic pollutants on Ag_3PO_4/ZnO nanowires using visible light and ultrasonic." Applied Surface Science **528**: 146819.
Yulizar, Y., R. Bakri, D. O. B. Apriandanu and T. Hidayat (2018). "ZnO/CuO nanocomposite prepared in one-pot green synthesis using seed bark extract of Theobroma cacao." Nano-Structures & Nano-Objects **16**: 300-305.
Zahrim, A. Y. and N. Hilal (2013). "Treatment of highly concentrated dye solution by coagulation/flocculation–sand filtration and nanofiltration." Water Resources and Industry **3**: 23-34.
Zhang, J., J. Lv, K. Dai, Q. Liu, C. Liang and G. Zhu (2017). "Facile and green synthesis of novel porous g-C_3N_4/Ag_3PO_4 composite with enhanced visible light photocatalysis." Ceramics International **43**(1): 1522-1529.
Zhang, Q., X. Li, Q. Zhao, Y. Shi, F. Zhang, B. Liu, J. Ke and L. Wang (2015). "Photocatalytic degradation of gaseous toluene over bcc-In_2O_3 hollow microspheres." Applied Surface Science **337**: 27-32.
Zhang, S., X. Gu, Y. Zhao and Y. Qiang (2015). "Effect of annealing temperature and time on structure, morphology and visible-light photocatalytic activities Ag_3PO_4 microparticles." Materials Science and Engineering: B **201**: 57-65.
Zhang, Z., J. B. Yi, J. Ding, L. M. Wong, H. L. Seng, S. J. Wang, J. G. Tao, G. P. Li, G. Z. Xing, T. C. Sum, C. H. Alfred Huan and T. Wu (2008). "Cu-Doped ZnO Nanoneedles and Nanonails: Morphological Evolution and Physical Properties." The Journal of Physical Chemistry C **112**(26): 9579-9585.
Zhou, Q., N. Yang, Y. Li, B. Ren, X. Ding, H. Bian and X. Yao (2020). "Total concentrations and sources of heavy metal pollution in global river and lake water bodies from 1972 to 2017." Global Ecology and Conservation **22**: e00925.
Zhu, C., Y. Zhao, L. Fang, J. Zheng, P. Hu, Y. Liu, X. Cao, Z. Chen, W. Wu and M. Wu (2017). "N-doped carbon quantum dots/Ag_3PO_4 hybrid materials with improved visible light photocatalytic activity and stability." Materials Letters **188**: 304-307.
Zhu, K., N. R. Neale, A. F. Halverson, J. Y. Kim and A. J. Frank (2010). "Effects of Annealing Temperature on the Charge-Collection and Light-Harvesting Properties of TiO_2 Nanotube-Based Dye-Sensitized Solar Cells." The Journal of Physical Chemistry C **114**(32): 13433-13441.
Zhu, P., M. Duan, R. Wang, J. Xu, P. Zou and H. Jia (2020). "Facile synthesis of ZnO/GO/Ag_3PO_4 heterojunction photocatalyst with excellent photodegradation activity for tetracycline hydrochloride under visible light." Colloids and Surfaces A: Physicochemical and Engineering Aspects **602**: 125118.
Zhu, P., M. Hu, M. Duan, L. Xie and M. Zhao (2020). "High visible light response Z-scheme Ag_3PO_4 / g-C_3N_4 / ZnO composite photocatalyst for efficient degradation of tetracycline hydrochloride: Preparation, properties and mechanism." Journal of Alloys and Compounds **840**: 155714.